Published in final edited form as:

Mol Cell. 2022 October 06; 82(19): 3613–3631.e7. doi:10.1016/j.molcel.2022.08.021.

Tissue-specific *Grb10/Ddc* insulator drives allelic architecture for cardiac development

Aimee M. Juan[1], **Yee Hoon Foong**[1], **Joanne L. Thorvaldsen**[1], **Yemin Lan**[1], **Nicolae A. Leu**[2], **Joel G. Rurik**[3], **Li Li**[3], **Christopher Krapp**[1], **Casey L. Rosier**[1], **Jonathan A. Epstein**[1,3], **Marisa S. Bartolomei**[1,4,*]

[1]Epigenetics Institute, Department of Cell and Developmental Biology, Perelman School of Medicine, University of Pennsylvania, Philadelphia, PA, United States, 19104

[2]Department of Biomedical Sciences, Center for Animal Transgenesis and Germ Cell Research, University of Pennsylvania School of Veterinary Medicine, Philadelphia, Pennsylvania, United States, 19104

[3]Penn Cardiovascular Institute, Department of Medicine, Department Cell and Developmental Biology, Perelman School of Medicine, University of Pennsylvania, Philadelphia, PA, United States, 19104

[4]Lead contact

Abstract

Allele-specific expression of imprinted gene clusters is governed by gametic DNA methylation at master regulators called imprinting control regions (ICRs). Non-gametic or secondary differentially methylated regions (DMRs) at promoters and exonic regions reinforce monoallelic expression but do not control an entire cluster. Here, we unveil an unconventional secondary DMR that is indispensable for tissue-specific imprinting of two previously unlinked genes, *Grb10* and *Ddc*. Using polymorphic mice, we mapped an intronic secondary DMR at *Grb10* with paternal-specific CTCF binding [CBR2.3] that forms contacts with *Ddc*. Deletion of paternal CBR2.3 removed a critical insulator, resulting in substantial shifting of chromatin looping and ectopic enhancer-promoter contacts. Destabilized gene architecture precipitated abnormal *Grb10-*

*Correspondence: bartolom@pennmedicine.upenn.edu.

Author Contributions: A.M.J. and M.S.B. conceived the study and wrote the manuscript. A.M.J. and M.S.B. designed experiments and interpreted results. A.M.J. developed *Grb10-Ddc* locus specific assays, collected and analyzed the data. A.M.J., C.K. and J.L.T. performed mouse husbandry for all experiments. A.M.J. and C.L.R. carried our DNA and RNA extractions, genotyping and RNA expression analyses. A.M.J., C.L.R., C.K. and Y.H.F. performed DNA methylation analyses. A.M.J., Y.H.F. and J.L.T. performed dissections, nuclei isolation and Capture-C experiments. A.M.J. and N.A.L. developed the $Grb10^{en/1msb}$ (CBR2.3 deletion allele) and $Grb10^{en/2msb}$ (PME deletion allele) models. A.M.J., J.G.R., L.L. and J.A.E. performed and/or evaluated the heart histology. A.M.J. and J.L.T. performed adult muscle histology. A.M.J., Y.H.F. and Y.L. performed bioinformatics analyses. Y.L. performed mouse CTCF ChIP-seq motif orientation analyses. A.M.J. performed CTCF ChIP-qPCR experiments. All authors read and revised the manuscript.

Declarations of Interest: The authors declare no competing interests.

Diversity and Inclusion Statement: One or more of the authors of this paper received support from a program designed to increase minority representation in science. While citing references scientifically relevant for this work, we also actively worked to promote gender balance in our reference list.

Ddc expression with developmental consequences in heart and muscle. Thus, we redefine the *Grb10-Ddc* imprinting domain by uncovering an unconventional intronic secondary DMR that functions as an insulator to instruct the tissue-specific, monoallelic expression of multiple genes – a feature previously ICR-exclusive.

Graphical Abstract

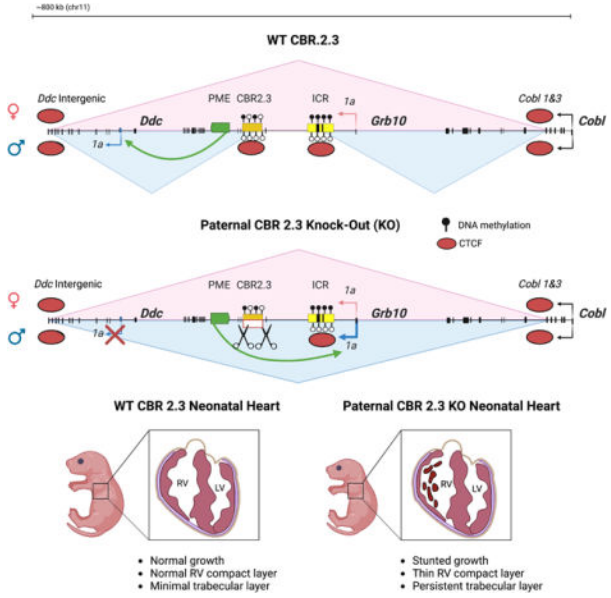

eTOC

Inherited monoallelic gene expression is governed by master regulatory elements known as imprinting control regions. Juan et al. describe an unconventional, developmentally unveiled, differentially methylated region that drives tissue-specific imprinting of *Grb10* and *Ddc* through the assembly of allele-specific CTCF-dependent architecture, thereby eliciting enhancer-promoter interactions in the developing heart.

INTRODUCTION

Diploid organisms have two sets of chromosomes and thereby inherit one gene copy from each parent, resulting in equal contributions of the parental genomes in offspring. However, a subclass of mammalian genes defies this law of inheritance. Termed imprinted genes, these ~200 genes are expressed from only one parental allele and reside in clusters. Imprinted genes “remember” parental origin by marking each allele in the germline with DNA methylation at discrete elements known as primary or gametic differentially methylated regions (gDMRs) or imprinting control regions (ICRs) (Barlow and Bartolomei, 2014; Ferguson-Smith, 2011). Maternal- or paternal-specific DNA methylation at ICRs is maintained after fertilization, despite the extensive epigenetic reprogramming that occurs at this time (Smith et al., 2012). Imprinted genes and DNA methylation at ICRs are critical for development of the embryo and placenta, as perturbations (including epimutations) at these elements often result in severe growth, neurological and metabolic disorders (Peters, 2014).

In addition to serving as a memory mark, one ICR controls the expression of all imprinted genes within a cluster by coordinating the activity of other linked regulatory elements such as noncoding RNAs and enhancers (Plagge, 2012; Singh et al., 2017; Sleutels et al., 2002; Thorvaldsen et al., 1998). Some ICRs bind the zinc finger protein CCCTC-binding factor (CTCF) that functions locally as an insulator to block ectopic enhancer-promoter contacts, and globally to construct chromatin compartments defined as topologically associated domains (TADs) (Dixon et al., 2012; Khoury et al., 2020; Prickett et al., 2013). Imprinted clusters have helped define CTCF-dependent insulators, as deletions or mutations in CTCF binding sites at ICRs reorganize gene architecture and trigger abnormal gene expression (Engel et al., 2008; Llères et al., 2019; Nativio et al., 2009; Naveh et al., 2021). Still, detailed allele-specific chromatin organization is lacking for most imprinted domains.

Several imprinted clusters also employ non-gametic or secondary differentially methylated regions (DMRs) as an additional layer of gene regulation. Distinct from ICRs, secondary DMRs also acquire allele-specific DNA methylation after implantation, but only a few have been identified and their regulatory roles are less clear (Nechin et al., 2019). Secondary DMRs typically localize to gene promoters/exonic regions and exhibit DNA methylation patterns that correlate with transcriptional silencing of proximal genes, exemplified by the *Cdkn1c*, *Gtl2* and *Nesp55* DMRs (Bhogal et al., 2004; Duart-Garcia and Braunschweig, 2013; Gagne et al., 2014; Guntrum et al., 2017; Jay et al., 1997; Nowak et al., 2011). For some loci, expression of imprinted genes is detected in blastocysts before secondary differential DNA methylation is established (Bhogal et al., 2004), suggesting that secondary DMRs arise as consequence of ICR-instructed genomic imprinting.

In this work, we investigated the imprinting mechanisms for two adjacent genes, *Growth factor receptor-bound protein 10* (*Grb10/GRB10*) and *dopa decarboxylase* (*Ddc/DDC*) that are located on mouse chromosome 11 and human chromosome 7. *Grb10* encodes multiple imprinted isoforms: a maternally expressed isoform from the *Grb10 1a* promoter that is abundant in heart and muscle, and two paternally expressed isoforms from the *1b1/1b2* promoters in neuronal lineages (Garfield et al., 2011; Hikichi et al., 2003; Plasschaert and Bartolomei, 2015; Sanz et al., 2008). *Ddc* also encodes multiple isoforms, including a biallelic isoform in the liver and kidney that initiates from exon 1 and a shorter isoform that originates from an alternative promoter ~8 kb downstream (Aguanno et al., 1996; Albert et al., 1992). Although the shorter isoform, *Ddc_Exon1a* (abbreviated here as *Ddc 1a*) is biallelically expressed in the brain, it is imprinted and paternally-expressed in the developing heart (Menheniott et al., 2008; Prickett et al., 2021). These imprinted, tissue-specific *Grb10* and *Ddc* isoforms are essential for mammalian development. Biallelic expression of *Grb10 1a* in mice results in reduced body growth and is linked to the human imprinting growth disorder Silver-Russell syndrome (SRS), while the loss of paternal *Grb10 1b* expression leads to neurobehavioral abnormalities (Dent et al., 2016; Joyce et al., 1999; Miyoshi et al., 1998; Rienecker et al., 2020; Shiura et al., 2009). Insufficient *Ddc* expression is associated with abnormal heart morphology, irregular heart rate and low blood pressure in mouse models of human DDC deficiency (Lee et al., 2009, 2013; Prickett et al., 2021). Thus, understanding how these genes are regulated is critical to human development and health.

Despite the exquisite mapping of imprinted *Grb10* and *Ddc* imprinted transcripts in different tissues, how the associated regulatory elements drive expression is largely unknown. Previous experiments have established that the *Grb10* ICR, which is methylated on the maternal allele and binds CTCF on the hypomethylated paternal allele, is essential for *Grb10* locus imprinting (Arnaud et al., 2003, 2006; Hikichi et al., 2003; Shiura et al., 2009). In contrast, the *Ddc* locus lacks a DMR that would confer parent-of-origin expression, indicating that a sequence elsewhere directs imprinted *Ddc 1a* (Menheniott et al., 2008). Thus, we investigated whether the tissue-specific imprinting of these adjacent genes is linked through a shared regulatory element that is distinct from the *Grb10* ICR. Here, we unveil an unconventional secondary DMR that organizes 3D chromatin and regulates tissue-specific imprinting of both *Grb10* and *Ddc*. Taking advantage of allelic polymorphisms in hybrid mice, we mapped a secondary DMR and CTCF binding sites to a *Grb10* intronic region we term **C**TCF **B**inding **R**egion **2.3** (CBR2.3). We demonstrate that CTCF preferentially binds to the hypomethylated paternal CBR2.3 allele, forming long-range paternal-specific contacts between *Grb10* and *Ddc*. This architecture enables CBR2.3 to function as a paternal-specific insulator, restricting the activity of a newly validated cardiac enhancer to the *Ddc 1a* promoter *in vivo*. Deletion of CBR2.3 from the paternal allele reorganized the topology of the imprinted domain, leading to ectopic enhancer-promoter interactions among imprinted promoters, resulting in biallelic *Grb10 1a* expression in muscular tissues and loss of *Ddc 1a* expression in the developing heart, overriding ICR regulation. Thus, our tissue-specific analysis uncovered a different type of regulatory element that is shared between the *Grb10* and *Ddc* genes, redefining them as one imprinted cluster. We show for the first time that a secondary DMR functions as a hierarchical equal to an ICR and use CBR2.3 as a modern paradigm for understanding genomic imprinting.

RESULTS

An intronic secondary DMR at *Grb10* binds CTCF on the paternal allele and forms paternal-specific chromatin loops with *Ddc*

To identify putative *cis* elements with high regulatory potential for *Grb10* and *Ddc* imprinting, we searched publicly available data from the mouse ENCODE project (Gorkin et al., 2020; Hsieh et al., 2020) (accession codes in Supp. Table 1). We scanned sequences near the *Grb10* ICR that also bound CTCF hypothesizing that genetic elements resembling the ICR also regulate genomic imprinting. We focused on a ~2.3 kb sequence positioned ~50 kb away from the ICR and within the second common intron of *Grb10* that contained two adjacent CTCF binding peaks. These colocalized with DNase hypersensitivity sites and cohesin (RAD21 and SMC3 subunits, Supp. Table 1), which is consistent with a putative architectural element (Fig. 1A). We termed this region CTCF Binding Region 2.3 (CBR2.3, genomic coordinates provided in Supp. Table 1). We also identified CTCF/cohesin binding sites near the 3' end of *Ddc* (termed *Ddc* Intergenic and *Ddc* 3') with CTCF motif orientations opposing CBR2.3, suggesting a potential long-range interaction (Rao et al., 2014) (Fig. 1A). Analysis of these genomic regions using public micro-C data (Hsieh et al., 2020) revealed a strong "corner dot" between the *Ddc* CTCF sites and CBR2.3, suggesting that these elements serve as endpoints for a contact domain. Similar long-range interactions

were found in human ESCs, indicating a conserved biological function of this domain (Supp. Fig. 1).

Notably, CBR2.3 resembles the *Grb10* ICR in several ways. CBR2.3 spans a GC-rich sequence and includes canonical CTCF binding site motifs that overlap CpGs, which if methylated may affect CTCF binding (Supp. Table 1). Because CTCF preferentially binds the hypomethylated paternal ICR, we characterized allele-specific DNA methylation at CBR2.3. Taking advantage of polymorphisms in hybrid mice, we performed targeted allele-specific bisulfite sequencing in F1 neonatal tissues generated from reciprocal matings between C57BL/6 (B6) and our in-house derived J11 mice with JF1/Ms sequence at the *Grb10* locus (Fig. 1B, additional details provided in the STAR Methods section). Whereas the maternal allele exhibited DNA methylation at >50% of all CpGs, the paternal allele was hypomethylated (4.5–6%), consistent with a newly identified DMR (Fig. 1C). Given the methylation-sensitive nature of CTCF binding (Engel et al., 2004; Hark et al., 2000), our allelic data strongly suggest that CTCF at CBR2.3 preferentially binds to the hypomethylated paternal allele, like the *Grb10* ICR.

We then asked if CTCF binding and differential DNA methylation at CBR2.3 were associated with allele-specific 3D chromatin, particularly involving *Ddc*. Using F1 hybrid wildtype (WT) tissues we performed allele-specific next-generation Capture-C, which maps long-range DNA interactions by pulling down chromatin with probes for regions of interest (Davies et al., 2016). From the viewpoint of 5’ CBR2.3, the paternal allele interacted with *Ddc* Intergenic, forming a ~150 kb paternal-specific loop (Fig. 1A, WT paternal vs WT maternal allele: $p < 0.001$; Supp. Table 5). This pronounced CBR2.3-*Ddc* looping interaction dominant on the paternal allele was confirmed using a probe anchored at *Ddc* Intergenic ($p < 10^{-6}$). Similar results were obtained for 3’ CBR2.3, *Ddc* 3’ and *Ddc* Mid (Supp. Fig. 1A; Supp. Table 5). Interestingly, the *Grb10* ICR was not involved in this architecture, which focused our attention to CBR2.3.

While CBR2.3-*Ddc* interactions were paternal-specific, a different architecture was observed on the maternal chromosome. The maternal *Ddc* Intergenic CTCF binding site interacted with two of four convergent CTCF sites at the *Cobl* gene (*Cobl* 1 & 3), which is located 5’ to *Grb10* and has an unclear imprinting status (Shiura et al., 2009) (Supp. Fig. 1A, $p < 10^{-6}$ and $p < 10^{-5}$, respectively). These CTCF sites formed a larger ~550 kb domain on the maternal allele. Altogether, these findings demonstrate that the *Grb10*, *Ddc* and *Cobl* loci are associated with distinct allelic gene architectures and provide the first direct evidence that these genes are spatially linked, redefining the region as an imprinted cluster.

To determine if the chromatin structure and methylation status of paternal CBR2.3 were consistent with paternal-specific CTCF binding, we performed allelic CTCF-ChIP followed by qPCR and pyrosequencing in F1 hybrid livers. Both CTCF peaks within CBR2.3 displayed preferential binding to the paternal allele (72% and 69%), reproducing the allele-specificity of the *Grb10* and *H19* ICRs and corroborating its regulatory potential (Fig. 1D) (Ideraabdullah et al., 2014). In contrast, *Ddc* CTCF sites exhibited biallelic binding patterns, consistent with the biallelic interactions described by Capture-C. We conclude that

CBR2.3 is a DMR with paternal-specific CTCF binding and allele-specific architecture at the *Grb10-Ddc* locus. Therefore, we focused on the regulatory properties of CBR2.3.

Paternal CBR2.3 functions as a tissue-specific insulator for allelic *Grb10-Ddc* expression

To investigate function, we constructed germline deletions of CBR2.3 using CRISPR/Cas9 (Fig. 2A, Supp. Fig. 2; details provided in the STAR Methods section). Heterozygotes (*CBR2.3*$^{\Delta/+}$) were mated with JF1 mice to generate maternal- and paternal-specific *CBR2.3* KO F1 hybrids [denoted as *CBR2.3*$^{\Delta/+}$ and *CBR2.3*$^{+/\Delta}$, respectively, wherein the maternal allele is listed first (Supp. Fig. 3A)]. ChIP-qPCR for CTCF at CBR2.3 revealed significantly less binding in *CBR2.3*$^{+/\Delta}$ tissues, which was consistent with paternal enrichment of CTCF observed in WT (Figs. 1D, 2B). In contrast, deletion of CBR2.3 on either allele had no effect on CTCF binding at *Ddc* or ICR, indicating that CTCF binding at these elements does not depend on CBR2.3 (Fig. 2B).

We next aimed to determine the role of CBR2.3 in *Grb10-Ddc* gene expression. In our mouse models, we focused on embryonic day 16 (**E16**) and postnatal day 2 (**P2**) hearts where *Grb10 1a* and *Ddc 1a* are co-expressed (Supp. Fig. 3B–C). Remarkably, total *Ddc 1a* expression was significantly decreased in *CBR2.3*$^{+/\Delta}$ hearts at both times compared to WT and *CBR2.3*$^{\Delta/+}$ (Fig. 2C). Total and allele-specific *Ddc 1a* was unperturbed with maternal deletion of CBR2.3, underscoring a paternal-specific effect (Fig. 2C, Supp. Fig. 3E–F). Notably, there was no compensation for the loss of imprinted *Ddc 1a* by the non-imprinted *Ddc* transcript or the biallelic isoform of *Ddc 1a* in the brain. In addition to the decrease in heart-specific *Ddc 1a* expression, *CBR2.3*$^{+/\Delta}$ mutants exhibited an increase in *Grb10 1a* expression levels in the developing heart and hindlimb muscle (Fig. 2D–E). We designed a targeted RNA pyrosequencing assay to measure allelic *Grb10 1a* expression ratios in these tissues (Yang et al., 2015). Although *Grb10 1a* is maternally expressed in WT, ~30–40% of transcripts were detected from the normally repressed paternal allele in *CBR2.3*$^{+/\Delta}$ heart and muscle, with a more robust loss of imprinting observed at E16 (Fig. 2F–G).

We next profiled additional tissues that express imprinted *Ddc 1a* and *Grb10* isoforms (Supp. Fig. 3D–I). *Ddc 1a* and *Grb10 1a* expression remained normal in all other tissues analyzed, including midbrain, placenta, intestine, liver and kidney, demonstrating a tissue- and paternal-specific effect. Neuronal tissues maintained normal paternal-specific *Grb10 1b1/2* expression, indicating that CBR2.3 does not regulate these isoforms. Taken together, the higher-order chromatin surrounding paternal CBR2.3 and opposing effects on cardiac *Grb10 1a-Ddc 1a* expression are consistent with the classic CTCF insulator model. Given its positioning between the imprinted promoters, CBR2.3 likely blocks paternal *Grb10 1a* gene activation from a local enhancer that activates *Ddc 1a*. We conclude that CBR2.3 functions as a shared, paternal- and tissue-specific insulator and define CBR2.3 as a newly identified regulatory element for the *Grb10-Ddc* imprinted locus.

CBR2.3 acquires differential DNA methylation during development, not in the germline

Of the tissues analyzed, only *CBR2.3*$^{+/\Delta}$ heart and skeletal muscle exhibited abnormal imprinted *Grb10 1a-Ddc 1a* expression. To understand this mechanism, we tested whether the differential DNA methylation at CBR2.3 was also tissue-specific. We performed targeted

bisulfite sequencing of both 5' and 3' CBR2.3 in various tissues of *CBR2.3*$^{\Delta/+}$ and *CBR2.3*$^{+/\Delta}$ neonatal mice, which allowed for the quantification of DNA methylation on the intact parental allele. The paternal CBR2.3 allele was significantly hypomethylated in all tissues tested (2–7%) whereas the maternal allele was consistently hypermethylated (Fig. 3A–C & 3E–F), indicating that CBR2.3 is not a tissue-specific DMR.

The allelic differences in DNA methylation at CBR2.3 across tissues recapitulate the parent-of-origin DNA methylation pattern at the *Grb10* ICR, suggesting that CBR2.3 may be a second ICR for the locus. To qualify as an ICR, the maternally methylated and paternally hypomethylated sequences at CBR2.3 must be established in the parental germlines (Abramowitz and Bartolomei, 2012). If the differential DNA methylation pattern persists throughout the genome-wide DNA demethylation that occurs after fertilization, then this region can be classified as an ICR (Andergassen et al., 2021; Li et al., 1993, 2008; Nakamura et al., 2007). To this end, we mapped DNA methylation levels of CBR2.3 in WT germ cells and blastocysts – a stage that coincides with global hypomethylation except at ICRs. Unlike the *Grb10* ICR, CBR2.3 was >95% methylated in both oocytes and sperm but was subsequently hypomethylated in the preimplantation embryo (Fig. 3D & 3G). Consistent with published data (Ruggeri et al., 2020), blastocysts exhibited low levels of DNA methylation at CBR2.3 (16–29%), indicating that gametic methylation at CBR2.3 is treated like the bulk genome. The differential DNA methylation pattern was established by E7.5, as embryos exhibited methylation for ~50% of DNA strands. These results illustrate that CBR2.3 is not an ICR but rather a secondary DMR that is developmentally controlled. This type of intronic, secondary DMR with the capacity to regulate multiple imprinted genes has not yet been described for an imprinted locus.

The proximity of secondary DMR CBR2.3 to the *Grb10* ICR prompted us to test whether deletion of CBR2.3 affected DNA methylation at the ICR. Bisulfite sequencing revealed the expected levels of DNA methylation for ICRs in CBR2.3 mutants (Fig. 3I), which was consistent with normal ICR CTCF binding (Fig. 2B). These results confirm that the ICR and CBR2.3 are distinct regulatory elements and that an intact ICR does not rescue *Grb10-Ddc* expression in *CBR2.3*$^{+/\Delta}$ heart and muscle. Until now, ICRs were known as the master regulatory elements for the monoallelic expression of imprinted genes within a cluster. Here, we define an unconventional secondary DMR that functions as a hierarchical equal to an ICR to regulate tissue-specific, imprinted gene expression.

Loss of paternal insulator CBR2.3 results in cardiac and muscular developmental defects

We next analyzed *CBR2.3*$^{\Delta/+}$ and *CBR2.3*$^{+/\Delta}$ mutants to determine if loss of *Ddc 1a* and/or biallelic *Grb10 1a* expression would precipitate heart and muscle defects. Although the tissue-specific roles of *Grb10 1a* and *Ddc 1a* in the heart and *Grb10 1a* in skeletal muscle are not completely known, imprinted genes are essential for the development of many organ systems (Plasschaert and Bartolomei, 2014; Tucci et al., 2019). *Ddc* encodes the protein AADC (aromatic L-amino acid decarboxylase) that catalyzes the synthesis of monoamine neurotransmitters dopamine and serotonin (Aguanno et al., 1996; Bucolo et al., 2019; Christenson et al., 1972; López-Sánchez et al., 2010; Prickett et al., 2021; Yavarone et al., 1993). Deletion of the serotonin 2B receptor or blocking serotonin uptake in the hearts

of mice results in decreased cardiomyocyte proliferation, noncompaction of the ventricular myocardium and poor septation, implicating the serotonin pathway and *Ddc* in cardiogenesis (Nebigil et al., 2000, 2001; Yavarone et al., 1993). In mice, *Ddc 1a* expression is highest at the time of birth and is localized to the right ventricle (Menheniott et al., 2008), therefore we focused on the developing heart wall in neonates.

Remarkably, *CBR2.3*$^{+/\Delta}$ hearts displayed a classic ventricular non-compaction phenotype with thin myocardium and a persistent trabecular layer that failed to condense into the underlying heart wall. The right ventricle was more affected than the left, which was consistent with the local expression pattern of *Ddc 1a* by immunofluorescence (Prickett et al., 2021) (Fig. 4A–B). Failed compaction of the right ventricular wall was indicated as early as E12.5 and became more pronounced by E15.5 when trabeculation has reached its peak (Captur et al., 2016) (Supp. Fig. 4A–C). As expected, *CBR2.3*$^{\Delta/+}$ right ventricular walls were not thin due to normal paternal *Ddc 1a* expression in maternal mutants. Single-cell RNA-sequencing of WT neonatal mouse hearts illustrated that *Grb10* and *Ddc* are co-expressed in developing and proliferating cardiomyocytes, suggesting that perturbation of both genes may contribute to ventricular non-compaction in *CBR2.3*$^{+/\Delta}$ hearts (Hu et al., 2018) (Fig. 4G). However, mouse models for total body knockout of *Ddc* revealed similar heart wall thinning, indicating that misexpression of *Ddc 1a* may be sufficient to drive this phenotype (Prickett et al., 2021).

GRB10 is a negative regulator of growth and is most abundant in tissues with high metabolic demand such as skeletal muscle. Maternal *Grb10* KO animals were previously shown to exhibit greater lean muscle relative to total body weight, likely due to the inhibitory effect of GRB10 on insulin signaling and glucose metabolism (Holt et al., 2012, 2018). Conversely, *CRB2.3*$^{+/\Delta}$ muscles exhibit biallelic *Grb10 1a* expression, which prompted us to test whether excess *Grb10 1a* negatively impacts body weight. Indeed, *CBR2.3*$^{+/\Delta}$ embryos were smaller in size, and neonates weighed less than their WT littermates without catch-up (Fig. 4C–D). Furthermore, adult *CBR2.3*$^{+/\Delta}$ lower limb muscle weights trended lower and centralized myofiber nuclei were detected, indicating myocyte death and attempted regeneration (Folker and Baylies, 2013) (Fig. 4E–F). These *in vivo* studies demonstrate that the allele- and tissue-specific insulator CBR2.3 is critical for normal heart and muscle development.

Paternal CTCF binding at *Grb10* DMR is required for allelic subTAD structuration *in vivo*

Our results showed CBR2.3 is secondary DMR that is involved in allelic gene architecture and behaves like an insulator to regulate imprinted *Grb10-Ddc* expression. To explore the mechanism underlying this “insulator effect,” we performed allele-specific Capture-C in *CBR2.3*$^{\Delta/+}$, *CBR2.3*$^{+/\Delta}$, WT$^{B6/JF1}$ and WT$^{JF1/B6}$ hybrid neonate hearts using probes for CBR2.3 and other putative regulatory sequences ($n = 3$ for each genotype, ~1 total billion read pairs for each sample, Supp. Table 3; details provided in the STAR Methods section). Deletion of paternal CBR2.3 disrupted the ~150 kb chromatin interacting domain between CBR2.3-*Ddc* Intergenic (paternal allele in WT vs *CBR2.3*$^{+/\Delta}$ $p < 10^{-6}$, Fig. 5A, Supp. Table 5). At the same time, “ectopic” interactions formed between paternal *Ddc* Intergenic and *Cobl* 1 & 3 CTCF binding sites, adopting a maternal-like chromatin architecture (*Cobl1:* $p < 10^{-5}$, *Cobl3:* $p < 10^{-4}$). Loss of the loop anchor in *CBR2.3*$^{+/\Delta}$ hearts was consistent with

loss of *Ddc 1a* expression and activation of normally silent paternal *Grb10 1a*, suggesting that CBR2.3 exerts its insulator function by forming distinct chromosomal domains for each promoter. As expected, $CBR2.3^{\Delta/+}$ hearts exhibited normal allelic interactions because CBR2.3 looping is paternal-specific (Fig. 5A–B). Identical results were observed in CBR2.3 mutant skeletal muscle (Supp. Fig. 5). These findings demonstrate that, like most insulators, CBR2.3 is a boundary element for a local subTAD and deletion of paternal CBR2.3 disrupts *Grb10-Ddc* expression by rewiring intradomain interactions (Fig. 5C).

We next investigated whether the changes in gene expression observed in $CBR2.3^{+/\Delta}$ hearts were associated with changes in architecture surrounding the ICR. In WT mice, the *Grb10* ICR formed loops with *Cobl* 1 & 3 CTCF sites exclusively on the paternal allele (Fig. 5A). These loops seem to isolate the upstream paternal *Grb10 1a* promoter to an intergenic domain without any regulatory elements and may contribute to paternal *Grb10 1a* silencing. Remarkably, deletion of paternal CBR2.3 resulted in a “weakening” of ICR-*Cobl* loop, creating an architecture that mimics the transcriptionally active maternal *Grb10* allele (Fig. 5A). The release of the ICR-*Cobl* interaction in $CBR2.3^{+/\Delta}$ hearts was coincident with biallelic *Grb10 1a* expression, indicating that relaxation of the subTAD boundary increases access to the normally silenced paternal *Grb10 1a* promoter. (Fig. 5B–C).

Next, we examined whether the ectopic interactions between *Grb10*, *Ddc*, and *Cobl* affected *Cobl* expression in $CBR2.3^{+/\Delta}$ heart and muscle. Two main *Cobl* transcripts are expressed, thus we designed primers for the long and short isoforms to track expression (Supp. Fig. 6A). In WT hearts, *Cobl* levels mimic *Grb10 1a* and *Ddc 1a* expression throughout development, but unlike *Grb10* and *Ddc*, *Cobl* is biallelic (Supp. Fig. 6B–C). Disruption of the *Grb10-Ddc-Cobl* architecture in $CBR2.3^{+/\Delta}$ hearts and muscle did not affect *Cobl* expression (Supp. Fig. 6D–G). Thus, our data illustrate that CTCF sites at the nearby *Cobl* gene serve an architectural purpose, while CBR2.3 functions as an insulator to promote imprinted *Grb10 1a* and *Ddc 1a* expression.

De novo interactions with newly validated cardiac enhancer upon subTAD reorganization

Having identified CBR2.3 as an insulator for the *Grb10-Ddc* cluster, we next investigated what regulatory element CBR2.3 was insulating. Insulators are well known to restrict enhancers to specific promoters within a spatial domain (Bell et al., 1999; Hark et al., 2000). Thus, we searched for a putative enhancer sequence within one megabase of CBR2.3 using publicly available ChIP-Seq data. We identified a sequence located in the fourth common *Grb10* intron we termed **p**utative **m**esoderm **e**nhancer or PME, positioned ~10 kb downstream of CBR2.3 (Fig. 6A). Unlike other sequences at the locus, PME overlapped with accessible chromatin and was enriched for active enhancer marks for developmental cardiac-specific enhancers (He et al., 2011, 2014; Zhou et al., 2017) (Fig. 6A, Supp. Fig. 7A–B). To understand how PME might communicate with local promoters, we performed allele-specific Capture-C in WT F1 hybrid hearts using PME as a viewpoint. These experiments revealed maternal-specific interactions with the *Grb10* promoter region, suggesting that PME may form enhancer-promoter (E-P) loops to activate maternal *Grb10 1a* (Fig. 6A, WT maternal vs WT paternal $p < 10^{-5}$). Interestingly, deletion of the paternal insulator CBR2.3 rearranged the paternal PME interactions to mimic the maternal allele,

as original interactions between PME and *Ddc* gene body were shifted to the *Grb10* promoter region (Fig. 6A, paternal allele WT vs $CBR2.3^{+/\Delta}$ $p < 0.01–0.001$, Supp. Table 5). These findings, together with the reciprocal changes in *Ddc 1a* and *Grb10 1a* expression in $CBR2.3^{+/\Delta}$ hearts, are consistent with paternal CBR2.3 serving as an insulator for the putative enhancer, PME.

To test whether PME is a functional enhancer for the *Grb10-Ddc* cluster, we deleted ~8.5 kb of the core sequence in mice (Fig. 6C; Supp. Fig. 7C) and mated heterozygous ($PME^{\Delta/+}$) male and female animals with B6 or JF1 mice to generate maternal- and paternal-specific enhancer KOs ($PME^{\Delta/+}$ and $PME^{+/\Delta}$, respectively) for total and allelic analyses. Remarkably, $PME^{+/\Delta}$ hearts exhibited a ~90% decrease in *Ddc 1a* expression, validating that paternal PME is a functional enhancer *Ddc 1a* in WT hearts (Fig. 6D). Together with our Capture-C data, these findings support the model that paternal CBR2.3-*Ddc* loops restrict PME activity to the *Ddc* domain. Although we could not detect the predicted paternal PME-*Ddc 1a* promoter interaction, these loops are likely too transient to be detected by the Capture-C approach used in this study (Hua et al., 2021). In contrast, maternal deletion of PME in heart and muscle had no effect on total *Grb10 1a* expression, supporting the presence of alternative enhancers that remain to be identified (Fig. 6E–F, 6H). An alternate enhancer may also explain the preserved cardiac development in $PME^{+/\Delta}$ mutants (Fig.4H–I). Finally, neither maternal nor paternal loss of PME activated *Ddc 1a* from the normally repressed allele (Fig. 6G), confirming PME as a *cis*-acting enhancer.

Paternal deletion of PME or CBR2.3 similarly disrupted *Ddc 1a* expression in the developing heart. However, unlike $CBR2.3^{+/\Delta}$ paternal loss of PME had no effect on *Grb10 1a* expression in heart or muscle (Fig. 6E–F, 6H). These results indicate that CBR2.3 functions independently from PME as a paternal insulator to maintain monoallelic *Grb10 1a* expression. Still, the proximity of CBR2.3 to PME (~10 kb) warranted the investigation of these sequences as a single bipartite element, an idea tested through the use of the deletion described above. If CBR2.3 and PME defined activity overlapped, then deletion of one element would affect the epigenetic modifications of the other. Paternal loss of CBR2.3 did not affect H3K27ac levels at PME (Supp. Fig. 7D, WT vs $CBR2.3^{+/\Delta}$, *Student's t-test*, $p = 0.55$), nor did deletion of PME affect the differential DNA methylation pattern at CBR2.3 (Fig. 3J, one-way ANOVA, $p = 0.32$). These data provide strong evidence that CBR2.3 and PME are not equal parts of a shared regulator. Instead, CBR2.3 is an insulator for a distinct cardiac enhancer, PME.

Disease-relevant GWAS SNPs in human orthologues of CBR2.3 and *Ddc*

Imprinted *GRB10* and *DDC 1A* expression is conserved in mice and humans (Blagitko et al., 2000; Prickett et al., 2021; Sanz et al., 2008) (Supp. Figs. 1 & 8). Similar regulatory elements and architecture suggest that humans may use comparable mechanisms for *GRB10-DDC* gene control. In particular, the PME in mice is orthologous to a human intronic region with strong cardiac enhancer potential, enriched with H3K27ac marks and intronic transcription suggestive of eRNAs (Spurrell et al., 2019) (Supp. Fig. 8). Consistent with our functional work in the mouse heart, GeneHancer algorithms predict human PME to interact with the *DDC 1A* promoter (Fishilevich et al., 2017). Interestingly,

human orthologues of CRB2.3, PME and *DDC* CTCF binding sites are enriched for single nucleotide polymorphisms that are associated with increased risk for heart failure (Aragam et al., 2019; Shah et al., 2020). These disease-related SNPs may interfere with *GRB10-DDC* loop anchors or tissue-specific enhancer-promoter activity, which in turn may contribute to heart pathology (Supp. Fig. 8, Supp. Table 4).

Discussion

While it is well understood that the genome is organized into large domains, relatively little is known about the finely-tuned chromatin architecture at individual loci in different cell types. There is ongoing debate as to how genome organization facilitates gene expression, as deletion of CTCF sites at TAD boundaries have unpredictable effects on local transcription. In this study, we provide a clear example of how chromatin architecture instructs gene expression in mammalian development using the imprinted *Grb10-Ddc* locus. Although imprinted genes are primarily governed by master regulators known as ICRs, our work using targeted deletions and hybrid mice uncovered a different type of secondary DMR and CTCF-dependent insulator (CBR2.3) at the *Grb10* locus that exerts similar levels of control. Consistent with the classic insulator model, CBR2.3 assembles allelic subdomains across the *Grb10-Ddc* locus, restricting newly validated cardiac enhancer PME to its cognate *Ddc 1a* promoter. *In vivo* deletion of paternal CBR2.3 rewired chromatin landscape to mimic the methylated maternal chromosome and maternal gene expression program, despite an intact ICR. We conclude that CBR2.3 overwrites the central *Grb10* ICR in a tissue-specific manner, breaking the paradigm of regulatory hierarchy between ICRs and DMRs that has been reported for other imprinted clusters. Moreover, our spatial analysis of *Grb10-Ddc* locus also revealed previously uncharacterized interactions with *Cobl*, which appear to provide a second layer of insulation for the paternal *Grb10 1a* promoter. Figure 7 summarizes our findings linking allele- and tissue-specific gene expression with chromatin organization for the *Grb10-Ddc-Cobl* locus and highlights CBR2.3 as the first direct, molecular link between these historically singleton imprinted genes.

GRB10-DDC locus in human health and disease

GRB10-DDC imprinting status is conserved in humans, with *GRB10* as a candidate gene for the imprinting disorder Silver-Russell syndrome (SRS), a growth restrictive disorder characterized by skeletal asymmetry and congenital heart disease (Blagitko et al., 2000; Cole and Levin, 1973; Ghanim et al., 2013; Patton, 1988; Prickett et al., 2021). Approximately 10% of all SRS cases occur in children who inherit two maternal copies of chromosome 7 (mUPD7), including the *GRB10-DDC-COBL* locus, resulting in double gene dosage of maternal *GRB10* and loss of paternal *DDC1A* in heart (Joyce et al., 1999; Miyoshi et al., 1998; Wakeling et al., 2017; Yuan et al., 2016). Orthologous CTCF binding sites, enhancers and topological domains within the *GRB10-DDC-COBL* locus suggest that humans likely use similar architecture found in mice to drive imprinted expression (Supp. Fig. 1). We speculate that mutations in these regulatory elements, particularly in the human orthologue for insulator CBR2.3, lead to heart or skeletal muscle pathologies resembling our observations in mice. Many studies examining the physiological roles of CTCF sites *in vivo* introduce sub-megabase sized deletions or inversions surrounding a TAD boundary, often

deleting nearby genes and regulatory elements (Amândio et al., 2021; Kraft et al., 2019; Lupiáñez et al., 2015). By precisely deleting 2.3 kb of intronic sequence at CBR2.3, we can attribute the developmental defects to a defined region that may be relevant to human health.

How is differential DNA methylation at CBR2.3 established?

The *Grb10* ICR is maternally methylated and the secondary DMR at CBR2.3 follows suit. During the blastocyst stage, CBR2.3 is largely hypomethylated and the region acquires a ~50% clonal DNA methylation pattern as early as E7.5. In postnatal tissues, CBR2.3 is finalized as a maternally methylated and paternally unmethylated DMR, with *Grb10 1a* expression originating from the methylated allele (Lopes et al., 2003; Takada et al., 2000). It is unknown how the maternal-specific DNA methylation at CBR2.3 is established from the hypomethylated state in the blastocyst. Mechanistic studies at other imprinted genes such as the *Gnas, Snrpn, Kcnq1, Zac1* and *U2af1-rs1 (Zrsr1)* point to a transcriptional elongation model for the establishment of maternal imprints in the oocyte via H3K36me3-dependent recruitment of DNMT3A/3L (Chotalia et al., 2009; Joh et al., 2018; Singh et al., 2017; Smith et al., 2011; Veselovska et al., 2015). These maternally methylated ICRs are often located in genomic regions that are actively transcribed, suggesting that transcription from an upstream promoter may contribute to their establishment. *Grb10* seems to fit this model for establishment of maternal imprints: CBR2.3 and ICR are respectively positioned ~60 kb and ~10 kb downstream from the *Grb10 1a* promoter that is active in oocytes and postnatal tissues (Chotalia et al., 2009; Shen et al., 2005; Veselovska et al., 2015). We hypothesize that maternal-specific *Grb10 1a* transcription recruits DNA methylation at both maternal DMRs. To test this hypothesis, independent deletions of the maternal *Grb10 1a* promoter and maternal *Grb10* ICR are required.

In summary, our *in* vivo analyses uncovered that developmentally-regulated, differential DNA methylation drives CTCF-mediated insulation for tissue-specific enhancer-promoter interactions at the *Grb10-Ddc* locus. Landmark studies that deleted or degraded CTCF *in vitro* showed minimal effects on gene expression, despite significant architectural changes (Nora et al., 2017; Zhang et al., 2020). These results are likely due to dormant cell-type or developmental stage-specific enhancers in the cell lines used. Here we profiled multiple neonatal mouse tissues at the *Grb10-Ddc* locus to discover that expression only in heart and muscle was affected, underscoring the importance of examining CTCF-dependent changes in a tissue-specific manner. We also highlight interactions in these tissues that were unreported in Hi-C studies using primary or immortalized cell lines (Hsieh et al., 2020), supporting the need to examine individual loci *in vivo*.

By probing for CBR2.3 on each parental chromosome in different tissues, we use *Grb10-Ddc* to model how allele- and tissue-specific elements regulate enhancer-promoter communication. Tissue-specific enhancers are rarely validated in developmental mouse models, with the *H19/Igf2* cluster being the classic example of a locus that uses allele-specific architecture and enhancers to promote imprinted gene expression (Kaffer et al., 2001; Leighton et al., 1995). The work described here for *Grb10-Ddc* locus illustrates that allele- and tissue-specific topology are not strictly required to be inherited by the germline like traditional imprinted loci. We show that a DMR that arises post-implantation can

assemble different chromosomal configurations to impact enhancer function and instruct allele-specific gene expression. In addition to defining an unconventional regulatory element for an imprinted locus, our results provide a mechanism for *cis*-acting genetic variation that may regulate expression of other tissue-specific autosomal genes. Given the genetic diversity and allelic skewing of many developmental and disease-related genes, we assert that this elegant regulatory framework is more prevalent in the genome than previously thought.

Limitations of study

Capture-C was only performed on heart and muscle and not in other tissues or at multiple developmental time points. With respect to enhancers, we only tested a single enhancer by deletion and there are more enhancers that drive expression of *Grb10* and *Ddc* in mesodermal tissues. We also did not conduct an extensive developmental phenotyping analysis of PME. Therefore, it is still somewhat difficult to disentangle the roles of *Grb10* and *Ddc* in the heart phenotype when the insulator is deleted.

STAR METHODS

RESOURCE AVAILABILITY

Lead contact—Further information and requests for resources and reagents should be directed to and will be fulfilled by the Lead Contact, Marisa Bartolomei (bartolom@pennmedicine.upenn.edu).

Materials availability—All unique/stable reagents, including CRISPR-generated mouse lines, used in this study are available from the Lead Contact with a completed Materials Transfer Agreement.

Data and code availability—The accession number for raw and processed Capture-C sequencing data reported in this paper is publicly available as of the date of publication and is deposited at GEO: GSE201519. Source data and image files for figures in the paper are available at Mendeley Data (https://data.mendeley.com/datasets/vmgpf62kxz/draft?a=3458285f-4067-417d-bc21-265ddc2f4065). This paper examined existing, publicly available data provided in the New WashU Epigenome Browser, visualized on the mouse mm10 genome. These accession numbers for the datasets are listed in Supplemental Table 1.

This paper does not report original code.

Any additional information required to reanalyze the data reported in this paper is available from the Lead Contact upon request.

EXPERIMENTAL MODEL AND SUBJECT DETAILS

Mouse husbandry and maintenance—All mice were housed in polysulfone cages in a pathogen-free facility on 12–12 light-dark cycle and had access to ad libitum water and standard chow (Laboratory Autoclavable Rodent Diet 5010, LabDiet. St. Louis, MO, USA). All animal work was conducted with the approval of the Institutional Animal Care and Use Committee at the University of Pennsylvania (Protocol Number: 804211).

Generation of wildtype hybrid mice for SNP analysis—Japanese Fancy mice JF1/MsJ (JF1) (Takada et al., 2013) (Stock# 003720) and C57BL/6J (B6) (Stock# 000664) mice were purchased from the Jackson Laboratory. J11 mice homozygous for JF1 sequence at *Grb10/Ddc* locus were generated as follows: (1) JF1 were crossed to B6 mice, (2) F1 progeny were back-crossed to B6 mice, (3) F2 progeny were then intercrossed to isolated mice homozygous for JF1 sequence at and within D11Mit129 and D11Mit224 markers (J11 were used in addition to JF1 mice to facilitate retrieval of hybrid *Grb10/Ddc* locus progeny). Hsd:NSA (CF-1) mice were purchased from Envigo (Strain Code# 033).

Generation of gene-edited mice—Intronic *Grb10* sequences CBR2.3 and PME were deleted *in vivo* using CRISPR-Cas9 editing in the B6 and B6D2strain as previously described (Miura et al., 2018; Wang et al., 2013). Briefly, pairs of sgRNAs were designed to target upstream and downstream of the CBR2.3 and enhancer sequences to be deleted using CRISPOR (Concordet and Haeussler, 2018) (http://crispor.tefor.net), Benchling (https://www.benchling.com/) and CHOPCHOP (Labun et al., 2019). For CBR2.3, sgRNAs were generated using a modified version of a previously published oligo assembly protocol (Yang et al., 2014). In this process an oligo encoding a T7 promoter, the guide RNA sequence and a short sequence from the PX335 backbone (5’ TTAATACGACTCACTATAGGNNNNNNNNNNNNNNNNNNgttttagagctagaaatagc-3’) were annealed to a second, generic oligo that includes complementary PX335 backbone sequence using Phusion HF PCR Kit (NEB, E0553S). The guide RNA was synthesized using HiScribe T7 Quick High Yield RNA Synthesis kit (NEB, E2040S) and purified using the MEGAclear Transcription Clean-up kit (Ambion, AM1908) prior to quantification using the Agilent RNA 6000 Nano kit. A mix containing Cas9 mRNA (Trilink, L-6125, final concentration of 100 ng/ul) and 2 sgRNAs (50 ng/uL each) in an injection buffer (10 mM Tris, pH 7.5; 0.1 mM EDTA) was injected into the pronucleus of B6 × B6D2 mouse embryos at the single-cell stage. For PME deletions, the EASI-CRISPR approach was employed (Miura et al., 2018) using Cas9 protein (IDT), crRNA designed with the CRISPR-Cas9 guide RNA design checker webtool from IDT (https://www.idtdna.com/site/order/designtool/index/CRISPR_SEQUENCE). crRNA and pre-prepared tracrRNA (IDT: Alt-R CRISPR-Cas9 tracrRNA) were resuspended with injection buffer to a final concentration of 1 ug/uL, mixed at a 1:2 ratio and annealed at 95°C (−2°C/s) to room temperature. Cas9 protein and crRNAs were added to 100 uL of injection mix at final concentrations of 20 ng/uL and 50 ng/uL, respectively, and filtered (Millpore UFC30VV25) by spinning at 12,000g for 2 minutes prior to injection.

All embryos used to generate the transgenic mice were collected from 6–8 week old B6 females which were super-ovulated via intraperitoneal injection (IP) using 5 IU of pregnant mare serum gonadotropin (PMSG) followed 48 hours later by 5 IU of human chorionic gonadotropin (hCG), after which they were mated to B6D2 studs. The B6D2 studs were generated by mating B6 females to DBA/2J males. The mosaic founders obtained from the CRISPR injection were 75% B6. Swiss Webster females were used as recipients and they were synchronized by using vasectomized males. After collection, embryos were incubated at 37C, 5% CO_2 incubator using KSOM media (Millipore, MR-202P-5F) covered with mineral oil (Millipore, ES-005-C) to prevent evaporation. All the microinjections, embryo

collection and embryo transfers were performed at room temperature using CZB-HEPES media. The zygotes used for CRISPR injections were collected 13–16 hours post hCG from the ampulla of the oviduct. To remove the cumulus cells from the zygotes, the zygote/cumulus cell complexes were cultured for 2–3 minutes at room temperature in CZB-HEPES media supplemented with 3 mg/ml hyaluronidase. Using a glass capillary tubing with filament (Cat# GC100TF-15), the CRISPR solution was microinjected into the cytoplasm about 2–3 hours after collection. The injected embryos were further incubated for 2–3 hours before they were transferred into the oviducts of E-0.5 pseudo-pregnant recipient females. All the glass capillaries were pulled using a Micropipette puller model #P-97. The injecting pressure was applied using an Eppendorf Cell Tram Air syringe and the entire procedure was performed using an inverted Nikon Eclipse microscope. F0 founder mice were identified from DNA isolated from ear punch, as described below. Deletions were validated in second generation F1 animals, and heterozygous animals were crossed to generate homozygous and heterozygous animals for breeding. Two founder lines were established for CBR2.3 and 3 founder lines for PME.

CBR2.3 (MGI: *Grb10*^{em1msb}) and PME (MGI: *Grb10*^{em2msb}) deletion mice were generated in-house and backcrossed to B6 mice for expression analyses. Male and female heterozygotes were bred with JF1 mice for allele-specific analyses in progeny. J11 mice were mated with male and female homozygote CBR2.3 animals for allele-specific Capture-C analysis in nuclei of progeny.

Timed matings—Embryonic day (E) was determined by checking for a vaginal sperm plug; E0.5 was taken to be 12.00 h (noon) on the day the plug was observed. Embryos were also visually staged upon dissection.

Dissections—For embryonic timepoints, dams were sacrificed by cervical dislocation and anesthetized on ice before organ collection. Pups were decapitated and the following tissues were collected: midbrain, cortex, kidney, liver, placenta, hindlimb muscle and lower two-thirds of the heart (to enrich for ventricles by removing atria and major vessel contamination). E16 hindlimbs were collected in lieu of hindlimb muscle in P2 animals.

Germ cell collection—For oocyte collection, 28 day-old CF-1 females were super-ovulated using standard gonadotropin protocols (Behringer et al., 2014). Pools of 20–100 germinal vesicle stage oocytes were collected from each ovary according to previous protocols (SanMiguel et al., 2018). Briefly, cumulus cells were removed from oocytes by mouth pipetting and transferring into clean drops of M2 medium (Sigma-Aldrich, M7167). When necessary, oocytes were briefly incubated in a drop of M2 medium containing a final concentration of 0.3 mg/ml hyaluronidase to remove cumulus cells. Oocytes were snap frozen in liquid nitrogen.

Sperm collection was performed as previously described (SanMiguel et al., 2018). Briefly, adult male mice >8 weeks of age were mated with a female for at least two days and then isolated for at least two days. After sacrifice, the epididymis was dissected. Epididymal sperm was collected on a needle and then incubated in room temperature PBS. Motile sperm were collected by removing the supernatant. Sperm were counted on a hemocytometer and

then pelleted [10 min at 12,000 rpm (13,523 g)]. The PBS was removed and the sperm pellet was snap frozen in liquid nitrogen.

METHOD DETAILS

CTCF motif orientation analysis—CTCF motif orientation was determined using the PWMScan – Genome Position Weight Matrix (PWM) scanner (https://ccg.epfl.ch/pwmscan/) (Ambrosini et al., 2018) and CTCF consensus sequence MA0139.1 from JASPAR (Khan et al., 2018) to extract the matching score for the best motif instance at each binding site. Human CTCF motif orientation was also determined with PWMScan and confirmed using pre-loaded CTCF ChIP-Seq data sets in GM12878 cell lines by Rao et al., 2014 in the JuiceBox visualization software (Robinson et al., 2018). Motifs of interest are annotated with CpGs in Supp. Table 1.

DNA isolation and genotyping of CRISPR-generated mice—DNA was isolated in a similar manner for genotyping, bisulfite sequencing and southern blot analysis. Embryonic (late gestation), neonatal and adult tissues, samples were first digested in lysis buffer (50mM Tris, pH8.0, 100mM EDTA, 0.5% SDS) with proteinase K (Sigma-Aldrich) overnight at 55°C. Genomic DNA was isolated using Phenol:Chloroform:Isoamyl Alcohol (Sigma-Aldrich P3803) and ethanol precipitation. DNA samples resuspended in TE were stored at 4°C. Sperm DNA was isolated using previously described methods (SanMiguel et al., 2018). The targeted alleles for CBR2.3 and PME deletions were validated in founder animals using Southern blot as previously described (Thorvaldsen et al., 1998), with restriction enzymes and probes indicated in Supp. Figures 2 and 6 and Supp. Table 2. For genotyping mutant CBR2.3 and PME alleles, primers spanning the desired deletion region were used (listed in Supp. Table 2), with 10 ng DNA and GoTaq Green Master Mix for PCR (Promega, M7121). Animals harboring the deleted regions were mapped using Sanger sequencing (Supp. Figures 2 and 6).

Targeted DNA methylation of regulatory elements using bisulfite-sequencing —Targeted DNA methylation analyses were performed according to Klobučar et al. (Klobučar et al., 2020). For neonatal tissues and sperm, ~2000 ng of gDNA was subjected to bisulfite mutagenesis using the Epitect kit (Qiagen) according to the manufacturer's protocol. For oocytes (30–100), blastocysts (20) and E7.5 embryos, samples were directly bisulfite treated using the Epitect Fast kit (Qiagen). 1–2 uL of bisulfite-mutagenized DNA was used per PCR for targeted bisulfite sequencing of select *Grb10* regions using PyroMark PCR kit (QIAGEN, 978703) and 1 uM of forward and reverse bisulfite primers. For primer design, genomic DNA sequences of the regions of interest were obtained from UCSC Genome Browser (https://www.genome.ucsc.edu) and imported into MethPrimer (https://www.urogene.org/methprimer/) (Li and Dahiya, 2002) or BiSearch (http://bisearch.enzim.hu/) (Tusnády et al., 2005) with the following criteria: optimal size 300 bp, a minimum of 5 CpGs in the PCR product, and no CpGs within the PCR primers. Primers are listed in Supp. Table 2. The following sequence was added to the forward (CTACACGACGCTCTTCCGATCT) and reverse (TGCTGAACCGCTCTTCCGATCTNNNNNNNN) primers (where N denotes a random nucleotide to generate a unique molecular identifier -UMI). Amplified regions were pooled

for column purification (Thomas Scientific, CM-500-50) with 2–3 regions per pool, for a total of 50 ng DNA, and the purified pools were barcoded with indexing primers using a Multiplex PCR Kit (QIAGEN, 246145). All indexed pools for a given sample were then pooled once more for column purification, after which library quality was determined using a Bioanalyzer DNA High Sensitivity chip (Agilent). Finally, all indexed libraries were pooled and sequenced on an Illumina MiSeq using a MiSeq Reagent Nano Kit v2 (500 cycles) (Illumina) using 10% PhIX spike-in as the libraries are of low complexity.

Targeted bisulfite sequencing analysis—Sequenced reads were trimmed to remove adapters using Trim Galore (version 0.6.2, http://www.bioinformatics.babraham.ac.uk/projects/trim_galore) and Cutadapt version 2.3). All the downstream steps were carried out in the IMPLICON pipeline (https://github.com/FelixKrueger/IMPLICON#step-i-umi-handling) (Klobučar et al., 2020). Trimmed reads were aligned to the mouse mm10 genome or a masked hybrid B6/JF1 genome (prepared with the SNPsplit package, version 0.3.4, https://github.com/FelixKrueger/SNPsplit) in paired-end mode with Bismark version 0.22.3, https://www.bioinformatics.babraham.ac.uk/projects/bismark). For hybrid B6/JF1 samples, reads were split allele-specifically with SNPsplit. CpG methylation calls were extracted from the mapped output using the Bismark Methylation Extractor to calculate percent methylation at each CpG with ≥ 30x coverage. For strand-specific analyses **CpG context files were checked against an annotated** probe file for each CpG contained within the amplicon. With modified Python and R scripts provided by Felix Krueger, the methylation state was extracted/visualized at the gene level, thus preserving DNA methylation status from each CpG on each DNA strand. Downstream analysis was performed using Excel and GraphPad (Prism).

RNA isolation, cDNA synthesis and RT-qPCR of mouse tissues—Mouse tissues were homogenized using mortar, pestle, syringe and 28-gauge needle in DNA/RNA Shield Buffer provided by ZYMO *Quick*-RNA Miniprep Plus (R1057). RNA was isolated according to the manufacturer's instructions. cDNA was synthesized using Superscript IV reverse transcriptase (Invitrogen) and random primers (Roche). Product from cDNA synthesis without RT enzyme was used as a negative control to confirm the absence of genomic DNA. For qRT-PCR assay, Power SYBR Green mater mix (Applied Biosystems) and primers in final concentration of 0.2μM were used on an ABI 7300 machine. Each sample was run in triplicate, and the mean value of triplicate plotted in graphs. 5ng of cDNA was used per reaction. For each primer set, reaction efficiency (E) was calculated using standard curve, and E^{-Ct} value of each gene was normalized to geometric mean of E^{-Ct} values of housekeeping genes. For mouse tissue samples, *Nono* and *Rpl13a* were used for normalization. Primers are listed in Supp. Table 2.

Allele-specific expression analyses of mouse tissues—For *Ddc 1a* allele-specific expression, restriction fragment length polymorphism analysis (RFLP) was used. 10–25 ng of cDNA was used for RT-PCR. PCR products were digested with restriction enzyme MspI (NEB, R0106S) for 2 hours at 37°C, and then run on 12% polyacrylamide gels. PCR product digests using pure B6 and JF1 strain cDNA were run together as controls for complete digestion. Images were analyzed using FIJI (Schindelin et al., 2012) (v2.0.0)

to quantify the band densitometry. For *Grb10 1a/1b1/1b2* isoforms, Pyrosequencing for Imprinting Expression (PIE) was used according to Yang and Calabrese et al. (Calabrese et al., 2015; Yang et al., 2015). Briefly, one cDNA product for each imprinted transcript was amplified using Apex Taq (Bioresearch Products, 42–138) with final primer concentrations at 0.2 uM, one of which was biotinylated. 8–12 uL of PCR product was sequenced on the PyroMark Q96 MD Pyrosequencer (Biotage, AB), using PyroMark Gold Q96 CDT Reagents (QIAGEN), and Streptavidin Sepharose beads (GE Healthcare). Quantification of allele-specific expression was performed using PyroMark Q96 MD software based on the presence of a SNP in the cDNA amplicon. Stacked bar charts were generated using RStudio (v1.4). Primers are listed in Supp. Table 2.

Nuclei isolation of heart and muscle tissues—Nuclei were isolated from fresh neonate mouse hearts (for Capture-C and CTCF ChIP-qPCR) harboring the CBR2.3 deletion. WT neonate B6xJF1 and JF1xB6 frozen livers were also used for allelic CTCF ChIP-qPCR. Tissues were finely chopped on ice and dounced in 10 mL of ice-cold homogenization buffer (10 mM Tris-HCl, pH 8.0; 5 mM $CaCl_2$; 3 mM $MgAc_2$; 0.32M sucrose; 0.1% Triton-X; 0.1 mM EDTA, 1X Protease Inhibitor cocktail (Roche); 1 mM DTT; 0.1 mM PMSF) 21 times with loose-fitting pestle and 14 times with tight-fitting pestle to release nuclei. Nuclei were fixed with 1% formaldehyde for 10 minutes at room temperature and quenched using 0.125 mM (final concentration) glycine for an additional 5 minutes. Nuclei were filtered through a series of cell strainers (100 uM, 70 uM, 40 uM and 20 uM) to clear debris. The nuclear pellet was washed with 50 mL ice-cold PBS and centrifuged at 500 × g for 15 minutes at 4°C before being snap frozen in liquid N_2.

Next generation Capture-C sequencing—Capture-C was performed as previously described (Davies et al., 2016). Briefly, heart and muscle tissues were obtained from wildtype neonate hearts of reciprocal F1 C57BL/6 (B6) and Japanese Fancy for chromosome 11 (J11) F1 hybrid mice, and J11 mice bred to male or female *CBR2.3*$^{\Delta/\Delta}$ mice to generate maternal- and paternal-specific CBR2.3 KO F1 hybrids (*CBR2.3*$^{\Delta/+}$ and *CBR2.3*$^{+/\Delta}$, respectively). 3C libraries were generated from nuclei using standard methods (Naveh et al., 2021) and *DnpII* as the primary restriction enzyme. Before oligonucleotide capture, 3C libraries were fragmented to 200–1000 bp sizes using a second digestion with two spike-ins of *NlaIII* overnight and in the morning for library prep and sequencing. The xGen Prism DNA library kit with primers (IDT 10006202 & 10005975) and adapters with unique molecular identifier (UMI) sequences were incorporated during adapter ligation to minimize sequence errors and reduce PCR duplication rates (IDT, 10006914). 1 ug of indexed samples were pooled before oligonucleotide capture using biotinylated oligonucleotides designed for the *Grb10* and *Ddc* promoters, CTCF binding sites and putative enhancer sequences using IDT Discovery Pool technology. Probe sequences are provided in Supp. Table 3. The first hybridization reaction included 5 pools of 4 samples (one of each genotype was included in each pool), with each hybridization pool set up using Mouse-COT DNA and 1.5 pM of Discovery Probes using reagents provided by the xGen Hybridization and Wash Kit according to the manufacturer's instructions (IDT, 1080577). After a 16-hour hybridization step, streptavidin bead pulldown (IDT, 1080577) and multiple bead washes using IDT xGen Hybridization and Wash Kit, PCR amplification of the captured material

was performed using KAPA HiFi HotStart Readymix Kit (KAPA Biosystems, KR0370) and library amplification primer (IDT, 1077676) for 14 cycles. A second capture was performed as above, with the exception that it was carried out with one-half of the Mouse-COT DNA and probe concentration used in the first capture. The material was sequenced using the Illumina NOVA-Seq platform with 250-bp paired end reads.

Bioinformatic analysis of the resulting reads contained two parts: removing duplicates using UMIs and implementing the CCseqBasicS pipeline. First, the beginning eight base pairs on the forward and reverse reads respectively were extracted using fgbio toolkit as UMIs (v0.5.0a, https://github.com/fulcrumgenomics/fgbio), which we later used for PCR duplication removal. Reads were then aligned to reference genome (mm10) using BWA MEM (v0.7.17) and default parameters. Only properly paired, primary alignments were kept for downstream analysis. Read pairs aligned to the same location which had the same UMI were removed as PCR duplicates using Picard (v2.18.15). The successfully aligned, non-duplicated read pairs were reverted to FASTQ format for Capture-C analysis using the CCseqBasicS (VS1.0.8) pipeline. FLASH (v1.2.11) was first used to merge paired-end reads from the same fragment, allowing the reads to overlap to a maximum of 250 bp (‘-M 150’). Fragments were digested with DpnII using the Python script implemented by the CCseqBasicS pipeline and mapped to mm10 reference genome using Bowtie (Langmead, 2010) (version 2.3.4.3) using default parameters and the maximum allowed insert size of 2000bp. Blacklist regions provided by the CCseqBasicS pipeline were excluded from the alignment file using bedtools toolkit (v.2.17.0). CCseqBasic tool (vCC5) was implemented with default settings (“--ampliconSize 2000 --noTrim -w 200 -i 20”) to acquire reporter reads of each designed captured probe in each sample. The tool was run in both non-SNP-specific as well as SNP-specific configurations (we designed probes so that they have B6/JF1 SNPs nearby to be sequenced; the list of used SNPs is available in Supp. Table 3). The final read counts for each probe region for each SNP are provided in Supp. Table 3. Bigwig files were generated for each sample and each probe by piling up all reads, B6 reads and JF1 reads separately, and then normalized to 10K reporter reads per designed probe for track visualization. We pooled reads from alleles in the same experimental group (WT-maternal, WT-paternal, CBR2.3 mKO-maternal and CBR2.3 pKO-paternal) together for contact site calling and visualization. For each experimental group and for each probe, contact sites were defined as peaks called using MACS2 (v2.1.1) with parameters “--nomodel --extsize 700 --qvalue 1e-100 --broad --nolambda --broad-cutoff 1e-100 --minsize 5000”. The corresponding contact site visualization, for each group and each probe, was defined by fourSig (Williams et al., 2014) with parameters “window.size=1, iterations=100, fdr=0.001, fdr.prob=0.05” and normalized to 100K reporter reads per designed probe for track visualization. Signal for each contact site was quantified on each bigwig file generated from the pipeline using bwtool (v1.0) (Pohl and Beato, 2014). Differential analysis between experiment groups was then performed using DESeq2 R package (FDR 0.05). Statistics for locus-specific comparisons are provided in Supp. Table 5. Figures were generated using .bw and .longinteraction files and visualized on WashU Epigenome Browser.

ChIP-qPCR—For nuclear sonication, all pellets were thawed on ice and resuspended at 1×10^6 cells per mL in sonication buffer (10 mM Tris-HCl, pH 8.0; 100 mM NaCl; 1

mM EDTA; 0.5 mM EGTA; 0.1% sodium deoxycholate; 0.5% N-lauroylsarcosine; 1X Protease inhibitor cocktail (Roche); 1 mM DTT; 0.1 mM PMSF) and sonicated using the Covaris S220 Focused-ultrasonicator for 20 minutes in 1 mL millTubes (140 Watts, 5% Duty Cycle, 200 bursts per second) to ~200 bp fragments. Samples were pooled to generate 3 replicates for each genotype with 5 ug of chromatin per IP, each of which was pre-cleared with 20 uL Protein G Dynabeads for 2 hours rotating at 4°C. Five percent of the total volume for each IP was taken for input measurements. Antibodies for CTCF (Cell Signaling, anti-rabbit D31H2), H3K27ac (Active Motif, anti-rabbit 39133) and IgG (Jacksonimmuno, anti-rabbit 011-000-003) were complexed to Protein G Dynabreads in 0.5% BSA for 6 hours at 4°C. Antibody-bead complexes were washed 3 times with blocking solution and incubated with pre-cleared chromatin overnight at 4°C. Samples were then washed with cold RIPA buffer (50 mM HEPES-KOH, pH 7.5; 500 mM LiCl; 1 mM EDTA; 1% NP40; 0.7% sodium-deoxycholate) for a total of 5 washes and resuspended in 1 mL ChIP Final Wash Buffer (10 mM Tris-HCl, pH 8.0, 1 mM EDTA; 50 mM NaCl). Beads were collected on a magnet to remove any residual buffer, resuspended in 200 uL ChIP Elution Buffer (50 mM Tris-HCl, pH 8.0; 10 mM EDTA; 1% SDS) and incubated at 65°C for 45 minutes on a thermomixer with gentle agitation (700 rpm) to elute chromatin. Input and IP samples were reverse-crosslinked at 65°C overnight using gentle rotation. The next morning, all samples were incubated with RNAse A (0.2 mg/mL final) at 37°C for 2 hours, followed by Proteinase K (0.2 mg/mL final) at 55°C for 2 hours. DNA was purified with phenol:chloroform:isoamyl alcohol, precipitated overnight at −20°C in high salt conditions and resuspended in 100 uL 1X TE buffer. Quantitative real-time qPCR was performed using the primers provided in Supp. Table 2 and Power SYBR Green Master Mix (Applied Biosystems) on a QuantStudio 7 Flex Real-Time PCR system. Relative CTCF binding was determined using the percent input calculation (Input % = $100*2^{\Delta Ct}$, where the ΔCt = Ct [ChIP] − (Ct [Input]− Log2 (Input Dilution Factor)).

Heart histology—For heart morphological analyses, tissues were fixed overnight in 4% paraformaldehyde and gradually dehydrated with ethanol. Hematoxylin and eosin (H&E) staining was performed according to a standard protocol. Images were obtained using a DMi8S widefield microscope equipped with 4X/0.13 HC PL FLUOTAR objective and DFC7000T color camera. Reported thickness of the ventricular compact and trabecular myocardium per mouse was the average of 3 individual measurements using ImageJ while blinded to genotype.

Muscle histology—For muscle, gastrocnemius and quadricep muscles were freshly dissected and frozen in cold isopentane according to a standard protocol (Kumar et al., 2015). 8–10 uM sections of frozen tissue were cut using Leica cryostat and stained with H&E according to Tichy et al. (Tichy et al., 2021). Images were taken using a DMi8S widefield microscope equipped with 4X/0.13 HC PL FLUOTAR objective and DFC7000T color camera with 10X/0.45 HC PL APO and 20X/0.80 HC PL APO objectives.

Human heart GWAS SNP analysis—Human data from the HERMES (Shah et al., 2020) and UK Biobank (Aragam et al., 2019) GWAS studies were accessed using the Cardiovascular Disease Knowledge Portal (CVDKP, https://cvd.hugeamp.org/). Heart-failure

related single nucleotide polymorphisms (SNPs) were identified by searching for the phenotype “heart failure” at the GRB10 gene. SNPs with significant p-values <0.05 and odds ratio (OR) >1 for a positive association with heart failure were used for downstream analysis. SNP positions were aligned to hg38 using UCSC Genome Browser and were overlaid with datasets for CTCF transcription factor binding (ENCSR825NXC) and RNA polymerase (Sloan et al., 2016) (Human ENCODE 3) and predicted human cardiac enhancers based on H3K27sc ChIP-Seq in human hearts (Spurrell et al., 2019) (GSE126571). Reported SNPs were categorized based on their relative location to annotated *cis* regulatory elements, within +/− 10 kb, and are provided in Supp. Table 4.

QUANTIFICATION AND STATISTICAL ANALYSIS

Unless otherwise stated, statistical analyses were carried out with Prism 9 (GraphPad Software). Unpaired, two-tailed *t* tests were applied when comparing methylation or expression between two groups. Comparisons of three or more groups were analyzed using an ordinary one-way analysis of variance (ANOVA) followed by Tukey’s multiple comparison post-hoc test if all means were compared or Brown-Forsythe if the medians of two groups were compared to WT controls, respectively. Error bars represent standard error of the mean. NG Capture-C experiments were performed on three biological replicates for each CBR2.3 genotype, with the exception of muscle with just one replicate for each genotype. Statistical significance in the differential analysis was calculated using DESeq2 as previously described (Davies et al., 2016; Love et al., 2014). Significance was defined as a p-value ≤ 0.05, unless otherwise stated. Details for the individual number of animals (n), litters and significance values can be found in the figure legends.

Supplementary Material

Refer to Web version on PubMed Central for supplementary material.

Acknowledgements:

This research was funded by grants from the National Institutes of Health, National Institute of Child Health and Human Development (5T32HD083185-02 and F31 HD095583-01A1 to A.M.J), National Institute of General Medicine (GM051279 to M.S.B) and National Heart, Lung and Blood Institute (R35 HL140018 to J.A.E). We thank Mayra Romero for technical assistance with pyrosequencing design and Isabel Sierra for contributions to CRISPR guide RNA design. We thank Eric Rhon-Calderon and Lisa Vrooman for assistance with oocyte and blastocyst collection. We thank Suhee Chang, Blake Caldwell, Rexxi Prassaya and Rob Plasschaert and other members of the Bartolomei lab for valuable discussions. We thank the Penn Center for Musculoskeletal Disorders Histology Core and Elisia Tichy for skeletal muscle histology protocols, tools and guidance. Figures were created with tracks from WashU and UCSC genome browsers, Adobe Illustrator, BioRender.com

References

Abramowitz LK, and Bartolomei MS (2012). Genomic imprinting: recognition and marking of imprinted loci. Curr Opin Genet Dev 22, 72–78. 10.1016/j.gde.2011.12.001. [PubMed: 22195775]

Aguanno A, Afar R, and Albert VR (1996). Tissue-specific Expression of the Nonneuronal Promoter of the Aromatic L-Amino Acid Decarboxylase Gene Is Regulated by Hepatocyte Nuclear Factor 1 (*). J Biol Chem 271, 4528–4538. 10.1074/jbc.271.8.4528. [PubMed: 8626808]

Albert VR, Lee MR, Bolden AH, Wurzburger RJ, and Aguanno A (1992). Distinct promoters direct neuronal and nonneuronal expression of rat aromatic L-amino acid decarboxylase. PNAS 98, 9508–9513. https://doi.org/10.1073.

Amândio AR, Beccari L, Lopez-Delisle L, Mascrez B, Zakany J, Gitto S, and Duboule D (2021). Sequential in-cis mutagenesis in vivo reveals various functions for CTCF sites at the mouse HoxD cluster. Biorxiv 2021.08.13.456193. 10.1101/2021.08.13.456193.

Ambrosini G, Groux R, and Bucher P (2018). PWMScan: a fast tool for scanning entire genomes with a position-specific weight matrix. Bioinformatics 34, 2483–2484. 10.1093/bioinformatics/bty127. [PubMed: 29514181]

Andergassen D, Smith ZD, Kretzmer H, Rinn JL, and Meissner A (2021). Diverse epigenetic mechanisms maintain parental imprints within the embryonic and extraembryonic lineages. Dev Cell 56, 2995–3005.e4. 10.1016/j.devcel.2021.10.010. [PubMed: 34752748]

Aragam KG, Chaffin M, Levinson RT, McDermott G, Choi SH, Shoemaker MB, Haas ME, Weng L-C, Lindsay ME, Smith JG, et al. (2019). Phenotypic Refinement of Heart Failure in a National Biobank Facilitates Genetic Discovery. Circulation 139, 489–501. 10.1161/circulationaha.118.035774.

Arnaud P, Monk D, Hitchins M, Gordon E, Dean W, Beechey CV, Peters J, Craigen W, Preece M, Stanier P, et al. (2003). Conserved methylation imprints in the human and mouse GRB10 genes with divergent allelic expression suggests differential reading of the same mark. Hum Mol Genet 12, 1005–1019. 10.1093/hmg/ddg110. [PubMed: 12700169]

Arnaud P, Hata K, Kaneda M, Li E, Sasaki H, Feil R, and Kelsey G (2006). Stochastic imprinting in the progeny of Dnmt3L−/− females. Hum Mol Genet 15, 589–598. 10.1093/hmg/ddi475. [PubMed: 16403808]

Barlow DP, and Bartolomei MS (2014). Genomic Imprinting in Mammals. Csh Perspect Biol 6, a018382. 10.1101/cshperspect.a018382.

Behringer, Gertsenstein M, and Nagy (2014). Mouse colony setup. In Manipulating the Mouse Embryo: A Laboratory Manual. Cold Spring Harbor, NY: Cold Spring Harbor Laboratory Press. 92–97..

Bell AC, West AG, and Felsenfeld G (1999). The Protein CTCF Is Required for the Enhancer Blocking Activity of Vertebrate Insulators. Cell 98, 387–396. 10.1016/s0092-8674(00)81967-4. [PubMed: 10458613]

Bhogal B, Arnaudo A, Dymkowski A, Best A, and Davis TL (2004). Methylation at mouse Cdkn1c is acquired during postimplantation development and functions to maintain imprinted expression. Genomics 84, 961–970. 10.1016/j.ygeno.2004.08.004. [PubMed: 15533713]

Blagitko N, Mergenthaler S, Schulz U, Wollmann HA, Craigen W, Eggermann T, Ropers H-H, and Kalscheuer VM (2000). Human GRB10 is imprinted and expressed from the paternal and maternal allele in a highly tissue- and isoform-specific fashion. Hum Mol Genet 9, 1587–1595. 10.1093/hmg/9.11.1587. [PubMed: 10861285]

Bucolo C, Leggio GM, Drago F, and Salomone S (2019). Dopamine outside the brain: The eye, cardiovascular system and endocrine pancreas. Pharmacol Therapeut 203, 107392. 10.1016/j.pharmthera.2019.07.003.

Calabrese JM, Starmer J, Schertzer MD, Yee D, and Magnuson T (2015). A Survey of Imprinted Gene Expression in Mouse Trophoblast Stem Cells. G3 Genes Genomes Genetics 5, 751–759. 10.1534/g3.114.016238. [PubMed: 25711832]

Captur G, Wilson R, Bennett MF, Luxán G, Nasis A, Pompa J.L. la, Moon JC, and Mohun TJ (2016). Morphogenesis of myocardial trabeculae in the mouse embryo. J Anat 229, 314–325. 10.1111/joa.12465. [PubMed: 27020702]

Chotalia M, Smallwood SA, Ruf N, Dawson C, Lucifero D, Frontera M, James K, Dean W, and Kelsey G (2009). Transcription is required for establishment of germline methylation marks at imprinted genes. Gene Dev 23, 105–117. 10.1101/gad.495809. [PubMed: 19136628]

Christenson JG, Dairman W, and Udenfriend S (1972). On the Identity of DOPA Decarboxylase and 5-Hydroxytryptophan Decarboxylase. Proc National Acad Sci 69, 343–347. 10.1073/pnas.69.2.343.

Cole RB, and Levin SE (1973). Congenital heart disease associated with the Russell-silver syndrome. South African Medical Journal = Suid-Afrikaanse Tydskrif Vir Geneeskunde.

Concordet J-P, and Haeussler M (2018). CRISPOR: intuitive guide selection for CRISPR/Cas9 genome editing experiments and screens. Nucleic Acids Res 46, gky354-. 10.1093/nar/gky354.

Davies JOJ, Telenius JM, McGowan SJ, Roberts NA, Taylor S, Higgs DR, and Hughes JR (2016). Multiplexed analysis of chromosome conformation at vastly improved sensitivity. Nat Methods 13, 74–80. 10.1038/nmeth.3664. [PubMed: 26595209]

Dent CL, Humby T, Lewis K, Plagge A, Fischer-Colbrie R, Wilkins JF, Wilkinson LS, and Isles AR (2016). Impulsive choices in mice lacking imprinted Nesp55. Genes Brain Behav 15, 693–701. 10.1111/gbb.12316. [PubMed: 27509352]

Dixon JR, Selvaraj S, Yue F, Kim A, Li Y, Shen Y, Hu M, Liu JS, and Ren B (2012). Topological domains in mammalian genomes identified by analysis of chromatin interactions. Nature 485, 376–380. 10.1038/nature11082. [PubMed: 22495300]

Downes DJ, Beagrie RA, Gosden ME, Telenius J, Carpenter SJ, Nussbaum L, Ornellas SD, Sergeant M, Eijsbouts CQ, Schwessinger R, et al. (2021). High-resolution targeted 3C interrogation of cis-regulatory element organization at genome-wide scale. Nat Commun 12, 531. 10.1038/s41467-020-20809-6. [PubMed: 33483495]

Duart-Garcia C, and Braunschweig MH (2013). The Igf2as Transcript is Exported into Cytoplasm and Associated with Polysomes. Biochem Genet 51, 119–130. 10.1007/s10528-012-9547-8. [PubMed: 23108799]

Engel N, West AG, Felsenfeld G, and Bartolomei MS (2004). Antagonism between DNA hypermethylation and enhancer-blocking activity at the H19 DMD is uncovered by CpG mutations. Nat Genet 36, 883–888. 10.1038/ng1399. [PubMed: 15273688]

Engel N, Raval AK, Thorvaldsen JL, and Bartolomei SM (2008). Three-dimensional conformation at the H19/Igf2 locus supports a model of enhancer tracking. Hum Mol Genet 17, 3021–3029. 10.1093/hmg/ddn200. [PubMed: 18617529]

Ferguson-Smith AC (2011). Genomic imprinting: the emergence of an epigenetic paradigm. Nat Rev Genet 12, 565–575. 10.1038/nrg3032. [PubMed: 21765458]

Fishilevich S, Nudel R, Rappaport N, Hadar R, Plaschkes I, Stein TI, Rosen N, Kohn A, Twik M, Safran M, et al. (2017). GeneHancer: genome-wide integration of enhancers and target genes in GeneCards. Database 2017, bax028. 10.1093/database/bax028.

Folker ES, and Baylies MK (2013). Nuclear positioning in muscle development and disease. Front Physiol 4, 363. 10.3389/fphys.2013.00363. [PubMed: 24376424]

Gagne A, Hochman A, Qureshi M, Tong C, Arbon J, McDaniel K, and Davis TL (2014). Analysis of DNA methylation acquisition at the imprinted Dlk1 locus reveals asymmetry at CpG dyads. Epigenet Chromatin 7, 9–9. 10.1186/1756-8935-7-9.

Garfield AS, Cowley M, Smith FM, Moorwood K, Stewart-Cox JE, Gilroy K, Baker S, Xia J, Dalley JW, Hurst LD, et al. (2011). Distinct physiological and behavioural functions for parental alleles of imprinted Grb10. Nature 469, 534–538. 10.1038/nature09651. [PubMed: 21270893]

Ghanim M, Rossignol S, Delobel B, Irving M, Miller O, Devisme L, Plennevaux J, Lucidarme-Rossi S, Manouvrier S, Salah A, et al. (2013). Possible association between complex congenital heart defects and 11p15 hypomethylation in three patients with severe Silver–Russell syndrome. Am J Med Genet A 161, 572–577. 10.1002/ajmg.a.35691.

Gorkin DU, Barozzi I, Zhao Y, Zhang Y, Huang H, Lee AY, Li B, Chiou J, Wildberg A, Ding B, et al. (2020). An atlas of dynamic chromatin landscapes in mouse fetal development. Nature 583, 744–751. 10.1038/s41586-020-2093-3. [PubMed: 32728240]

Guntrum M, Vlasova E, and Davis TL (2017). Asymmetric DNA methylation of CpG dyads is a feature of secondary DMRs associated with the Dlk1/Gtl2 imprinting cluster in mouse. Epigenet Chromatin 10, 31. 10.1186/s13072-017-0138-0.

Hark AT, Schoenherr CJ, Katz DJ, Ingram RS, Levorse JM, and Tilghman SM (2000). CTCF mediates methylation-sensitive enhancer-blocking activity at the H19/Igf2 locus. Nature 405, 486. 10.1038/35013106. [PubMed: 10839547]

He A, Kong SW, Ma Q, and Pu WT (2011). Co-occupancy by multiple cardiac transcription factors identifies transcriptional enhancers active in heart. Proc National Acad Sci 108, 5632–5637. 10.1073/pnas.1016959108.

He A, Gu F, Hu Y, Ma Q, Ye LY, Akiyama JA, Visel A, Pennacchio LA, and Pu WT (2014). Dynamic GATA4 enhancers shape the chromatin landscape central to heart development and disease. Nat Commun 5, 4907–4907. 10.1038/ncomms5907. [PubMed: 25249388]

Hikichi T, Kohda T, Kaneko-Ishino T, and Ishino F (2003). Imprinting regulation of the murine Meg1 / Grb10 and human GRB10 genes; roles of brain-specific promoters and mouse-specific CTCF-binding sites. Nucleic Acids Res 31, 1398–1406. 10.1093/nar/gkg232. [PubMed: 12595547]

Holt LJ, Turner N, Mokbel N, Trefely S, Kanzleiter T, Kaplan W, Ormandy CJ, Daly RJ, and Cooney GJ (2012). Grb10 regulates the development of fiber number in skeletal muscle. Faseb J 26, 3658–3669. 10.1096/fj.11-199349. [PubMed: 22623587]

Holt LJ, Brandon AE, Small L, Suryana E, Preston E, Wilks D, Mokbel N, Coles CA, White JD, Turner N, et al. (2018). Ablation of Grb10 Specifically in Muscle Impacts Muscle Size and Glucose Metabolism in Mice. Endocrinology 159, 1339–1351. 10.1210/en.2017-00851. [PubMed: 29370381]

Hsieh T-HS, Cattoglio C, Slobodyanyuk E, Hansen AS, Rando OJ, Tjian R, and Darzacq X (2020). Resolving the 3D Landscape of Transcription-Linked Mammalian Chromatin Folding. Mol Cell 78, 539–553.e8. 10.1016/j.molcel.2020.03.002. [PubMed: 32213323]

Hu P, Liu J, Zhao J, Wilkins BJ, Lupino K, Wu H, and Pei L (2018). Single-nucleus transcriptomic survey of cell diversity and functional maturation in postnatal mammalian hearts. Gene Dev 32, 1344–1357. 10.1101/gad.316802.118. [PubMed: 30254108]

Hua P, Badat M, Hanssen LLP, Hentges LD, Crump N, Downes DJ, Jeziorska DM, Oudelaar AM, Schwessinger R, Taylor S, et al. (2021). Defining genome architecture at base-pair resolution. Nature 1–5. 10.1038/s41586-021-03639-4.

Ideraabdullah FY, Thorvaldsen JL, Myers JA, and Bartolomei MS (2014). Tissue-specific insulator function at H19/Igf2 revealed by deletions at the imprinting control region. Hum Mol Genet 23, 6246–6259. 10.1093/hmg/ddu344. [PubMed: 24990148]

Jay P, Rougeulle C, Massacrier A, Moncla A, Mattei M-G, Malzac P, Roëckel N, Taviaux S, Lefranc J-LB, Cau P, et al. (1997). The human necdin gene, NDN, is maternally imprinted and located in the Prader-Willi syndrome chromosomal region. Nat Genet 17, 357–361. 10.1038/ng1197-357. [PubMed: 9354807]

Joh K, Matsuhisa F, Kitajima S, Nishioka K, Higashimoto K, Yatsuki H, Kono T, Koseki H, and Soejima H (2018). Growing oocyte-specific transcription-dependent de novo DNA methylation at the imprinted Zrsr1-DMR. Epigenet Chromatin 11, 28. 10.1186/s13072-018-0200-6.

Joyce CA, Sharp A, Walker JM, Bullman H, and Temple IK (1999). Duplication of 7p12.1-p13, including GRB10 and IGFBP1, in a mother and daughter with features of Silver-Russell syndrome. Hum Genet 105, 273–280. 10.1007/s004399900128. [PubMed: 10987657]

Kaffer CR, Grinberg A, and Pfeifer K (2001). Regulatory Mechanisms at the MouseIgf2/H19 Locus. Mol Cell Biol 21, 8189–8196. 10.1128/mcb.21.23.8189-8196.2001. [PubMed: 11689707]

Khan A, Fornes O, Stigliani A, Gheorghe M, Castro-Mondragon JA, Lee R. van der, Bessy A, Chèneby J, Kulkarni SR, Tan G, et al. (2018). JASPAR 2018: update of the open-access database of transcription factor binding profiles and its web framework. Nucleic Acids Res 46, D260–D266. 10.1093/nar/gkx1126. [PubMed: 29140473]

Khoury A, Achinger-Kawecka J, Bert SA, Smith GC, French HJ, Luu P-L, Peters TJ, Du Q, Parry AJ, Valdes-Mora F, et al. (2020). Constitutively bound CTCF sites maintain 3D chromatin architecture and long-range epigenetically regulated domains. Nat Commun 11, 54. 10.1038/s41467-019-13753-7. [PubMed: 31911579]

Klobučar T, Kreibich E, Krueger F, Arez M, Pólvora-Brandão D, von Meyenn F, da Rocha ST, and Eckersley-Maslin M (2020). IMPLICON: an ultra-deep sequencing method to uncover DNA methylation at imprinted regions. Nucleic Acids Res 48, gkaa567-. 10.1093/nar/gkaa567.

Kraft K, Magg A, Heinrich V, Riemenschneider C, Schöpflin R, Markowski J, Ibrahim DM, Acuna-Hidalgo R, Despang A, Andrey G, et al. (2019). Serial genomic inversions induce tissue-specific architectural stripes, gene misexpression and congenital malformations. Nat Cell Biol 21, 305–310. 10.1038/s41556-019-0273-x. [PubMed: 30742094]

Krueger F, and Andrews SR (2011). Bismark: a flexible aligner and methylation caller for Bisulfite-Seq applications. Bioinformatics 27, 1571–1572. 10.1093/bioinformatics/btr167. [PubMed: 21493656]

Krueger F, and Andrews SR (2016). SNPsplit: Allele-specific splitting of alignments between genomes with known SNP genotypes. F1000research 5, 1479. 10.12688/f1000research.9037.1. [PubMed: 27429743]

Kumar A, Accorsi A, Rhee Y, and Girgenrath M (2015). Do's and Don'ts in the Preparation of Muscle Cryosections for Histological Analysis. J Vis Exp e52793. 10.3791/52793. [PubMed: 26066009]

Labun K, Montague TG, Krause M, Torres Cleuren YN, Tjeldnes H, and Valen E (2019). CHOPCHOP v3: expanding the CRISPR web toolbox beyond genome editing. Nucleic Acids Res 47, W171–W174. 10.1093/nar/gkz365. [PubMed: 31106371]

Langmead B (2010). Aligning Short Sequencing Reads with Bowtie. Curr Protoc Bioinform 32, 11.7.1–11.7.14. 10.1002/0471250953.bi1107s32.

Lee H-F, Tsai C-R, Chi C-S, Chang T-M, and Lee H-J (2009). Aromatic l-amino acid decarboxylase deficiency in Taiwan. Eur J Paediatr Neuro 13, 135–140. 10.1016/j.ejpn.2008.03.008.

Lee N-C, Shieh Y-D, Chien Y-H, Tzen K-Y, Yu I-S, Chen P-W, Hu M-H, Hu M, Muramatsu S, Ichinose H, et al. (2013). Regulation of the dopaminergic system in a murine model of aromatic l-amino acid decarboxylase deficiency. Neurobiol Dis 52, 177–190. 10.1016/j.nbd.2012.12.005. [PubMed: 23275025]

Leighton PA, Saam JR, Ingram RS, Stewart CL, and Tilghman SM (1995). An enhancer deletion affects both H19 and Igf2 expression. Genes & Development 9, 2079–2089..

Li H (2013). Aligning sequence reads, clone sequences and assembly contigs with BWA-MEM. Arxiv.

Li L-C, and Dahiya R (2002). MethPrimer: designing primers for methylation PCRs. BIOINFORMATICS 18, 1427–1433. 10.1093/bioinformatics/18.11.1427. [PubMed: 12424112]

Li E, Beard C, and Jaenisch R (1993). Role for DNA methylation in genomic imprinting. Nature 366, 362–365. 10.1038/366362a0. [PubMed: 8247133]

Li X, Ito M, Zhou F, Youngson N, Zuo X, Leder P, and Ferguson-Smith AC (2008). A Maternal-Zygotic Effect Gene, Zfp57, Maintains Both Maternal and Paternal Imprints. Dev Cell 15, 547–557. 10.1016/j.devcel.2008.08.014. [PubMed: 18854139]

Llères D, Moindrot B, Pathak R, Piras V, Matelot M, Pignard B, Marchand A, Poncelet M, Perrin A, Tellier V, et al. (2019). CTCF modulates allele-specific sub-TAD organization and imprinted gene activity at the mouse Dlk1-Dio3 and Igf2-H19 domains. Genome Biol 20, 272. 10.1186/s13059-019-1896-8. [PubMed: 31831055]

Lopes S, Lewis A, Hajkova P, Dean W, Oswald J, Forné T, Murrell A, Constância M, Bartolomei M, Walter J, et al. (2003). Epigenetic modifications in an imprinting cluster are controlled by a hierarchy of DMRs suggesting long-range chromatin interactions. Hum Mol Genet 12, 295–305. 10.1093/hmg/ddg022. [PubMed: 12554683]

López-Sánchez C, Bártulos Ó, Martínez-Campos E, Gañán C, Valenciano AI, García-Martínez V, Pablo FD, and Hernández-Sánchez C (2010). Tyrosine hydroxylase is expressed during early heart development and is required for cardiac chamber formation. Cardiovasc Res 88, 111–120. 10.1093/cvr/cvq179. [PubMed: 20525643]

Love MI, Huber W, and Anders S (2014). Moderated estimation of fold change and dispersion for RNA-seq data with DESeq2. Genome Biol 15, 550. 10.1186/s13059-014-0550-8. [PubMed: 25516281]

Lupiáñez DG, Kraft K, Heinrich V, Krawitz P, Brancati F, Klopocki E, Horn D, Kayserili H, Opitz JM, Laxova R, et al. (2015). Disruptions of Topological Chromatin Domains Cause Pathogenic Rewiring of Gene-Enhancer Interactions. Cell 161, 1012–1025. 10.1016/j.cell.2015.04.004. [PubMed: 25959774]

Magoč T, and Salzberg SL (2011). FLASH: fast length adjustment of short reads to improve genome assemblies. Bioinformatics 27, 2957–2963. 10.1093/bioinformatics/btr507. [PubMed: 21903629]

Menheniott TR, Woodfine K, Schulz R, Wood AJ, Monk D, Giraud AS, Baldwin HS, Moore GE, and Oakey RJ (2008). Genomic Imprinting of Dopa decarboxylase in Heart and Reciprocal Allelic Expression with Neighboring Grb10▾. Mol Cell Biol 28, 386–396. 10.1128/mcb.00862-07. [PubMed: 17967881]

Miura H, Quadros RM, Gurumurthy CB, and Ohtsuka M (2018). Easi-CRISPR for creating knock-in and conditional knockout mouse models using long ssDNA donors. Nat Protoc 13, 195–215. 10.1038/nprot.2017.153. [PubMed: 29266098]

Miyoshi N, Kuroiwa Y, Kohda T, Shitara H, Yonekawa H, Kawabe T, Hasegawa H, Barton SC, Surani MA, Kaneko-Ishino T, et al. (1998). Identification of the Meg1/Grb10 imprinted gene on mouse proximal chromosome 11, a candidate for the Silver–Russell syndrome gene. Proc National Acad Sci 95, 1102–1107. 10.1073/pnas.95.3.1102.

Nakamura T, Arai Y, Umehara H, Masuhara M, Kimura T, Taniguchi H, Sekimoto T, Ikawa M, Yoneda Y, Okabe M, et al. (2007). PGC7/Stella protects against DNA demethylation in early embryogenesis. Nat Cell Biol 9, 64–71. 10.1038/ncb1519. [PubMed: 17143267]

Nativio R, Wendt KS, Ito Y, Huddleston JE, Uribe-Lewis S, Woodfine K, Krueger C, Reik W, Peters J-M, and Murrell A (2009). Cohesin Is Required for Higher-Order Chromatin Conformation at the Imprinted IGF2-H19 Locus. Plos Genet 5, e1000739. 10.1371/journal.pgen.1000739. [PubMed: 19956766]

Naveh NSS, Deegan DF, Huhn J, Traxler E, Lan Y, Weksberg R, Ganguly A, Engel N, and Kalish JM (2021). The role of CTCF in the organization of the centromeric 11p15 imprinted domain interactome. Nucleic Acids Res 49, gkab475-. 10.1093/nar/gkab475.

Nebigil CG, Choi D-S, Dierich A, Hickel P, Meur ML, Messaddeq N, Launay J-M, and Maroteaux L (2000). Serotonin 2B receptor is required for heart development. PNAS 97, 9508–9513. 10.1073/pnas.97.17.9508. [PubMed: 10944220]

Nebigil CG, Hickel P, Messaddeq N, Vonesch J-L, Douchet MP, Monassier L, György K, Matz R, Andriantsitohaina R, Manivet P, et al. (2001). Ablation of Serotonin 5-HT2B Receptors in Mice Leads to Abnormal Cardiac Structure and Function. Circulation 103, 2973–2979. 10.1161/01.cir.103.24.2973. [PubMed: 11413089]

Nechin J, Tunstall E, Raymond N, Hamagami N, Pathmanabhan C, Forestier S, and Davis TL (2019). Hemimethylation of CpG dyads is characteristic of secondary DMRs associated with imprinted loci and correlates with 5-hydroxymethylcytosine at paternally methylated sequences. Epigenet Chromatin 12, 64. 10.1186/s13072-019-0309-2.

Nora EP, Goloborodko A, Valton A-L, Gibcus JH, Uebersohn A, Abdennur N, Dekker J, Mirny LA, and Bruneau BG (2017). Targeted Degradation of CTCF Decouples Local Insulation of Chromosome Domains from Genomic Compartmentalization. Cell 169, 930–944.e22. 10.1016/j.cell.2017.05.004. [PubMed: 28525758]

Nowak K, Stein G, Powell E, He LM, Naik S, Morris J, Marlow S, and Davis TL (2011). Establishment of paternal allele-specific DNA methylation at the imprinted mouse Gtl2 locus. Epigenetics 6, 1012–1020. 10.4161/epi.6.8.16075. [PubMed: 21725202]

Patton MA (1988). Russell-Silver syndrome. J Med Genet 25, 557. 10.1136/jmg.25.8.557. [PubMed: 3050100]

Peters J (2014). The role of genomic imprinting in biology and disease: an expanding view. Nat Rev Genet 15, 517–530. 10.1038/nrg3766. [PubMed: 24958438]

Plagge A (2012). Non-Coding RNAs at the Gnas and Snrpn-Ube3a Imprinted Gene Loci and Their Involvement in Hereditary Disorders. Frontiers Genetics 3, 264. 10.3389/fgene.2012.00264.

Plasschaert RN, and Bartolomei MS (2014). Genomic imprinting in development, growth, behavior and stem cells. Development 141, 1805–1813. 10.1242/dev.101428. [PubMed: 24757003]

Plasschaert RN, and Bartolomei MS (2015). Tissue-specific regulation and function of Grb10 during growth and neuronal commitment. Proc National Acad Sci 112, 6841–6847. 10.1073/pnas.1411254111.

Pohl A, and Beato M (2014). bwtool: a tool for bigWig files. Bioinformatics 30, 1618–1619. 10.1093/bioinformatics/btu056. [PubMed: 24489365]

Prickett AR, Barkas N, McCole RB, Hughes S, Amante SM, Schulz R, and Oakey RJ (2013). Genome-wide and parental allele-specific analysis of CTCF and cohesin DNA binding in mouse brain reveals a tissue-specific binding pattern and an association with imprinted differentially methylated regions. Genome Res 23, 1624–1635. 10.1101/gr.150136.112. [PubMed: 23804403]

Prickett AR, Montibus B, Barkas N, Amante SM, Franco MM, Cowley M, Puszyk W, Shannon MF, Irving MD, Madon-Simon M, et al. (2021). Imprinted Gene Expression and Function of the Dopa Decarboxylase Gene in the Developing Heart. Frontiers Cell Dev Biology 9, 676543. 10.3389/fcell.2021.676543.

Rao SSP, Huntley MH, Durand NC, Stamenova EK, Bochkov ID, Robinson JT, Sanborn AL, Machol I, Omer AD, Lander ES, et al. (2014). A 3D Map of the Human Genome at Kilobase Resolution Reveals Principles of Chromatin Looping. Cell 159, 1665–1680. 10.1016/j.cell.2014.11.021. [PubMed: 25497547]

Rienecker KDA, Chavasse AT, Moorwood K, Ward A, and Isles AR (2020). Detailed analysis of paternal knockout Grb10 mice suggests effects on stability of social behavior, rather than social dominance. Genes Brain Behav 19. 10.1111/gbb.12571.

Robinson JT, Turner D, Durand NC, Thorvaldsdóttir H, Mesirov JP, and Aiden EL (2018). Juicebox.js Provides a Cloud-Based Visualization System for Hi-C Data. Cell Syst 6, 256–258.e1. 10.1016/j.cels.2018.01.001. [PubMed: 29428417]

Ruggeri E, Lira-Albarrán S, Grow EJ, Liu X, Harner R, Maltepe E, Ramalho-Santos M, Donjacour A, and Rinaudo P (2020). Sex-specific epigenetic profile of inner cell mass of mice conceived in vivo or by IVF. Mol Hum Reprod 26, 866–878. 10.1093/molehr/gaaa064. [PubMed: 33010164]

SanMiguel JM, Abramowitz LK, and Bartolomei MS (2018). Imprinted gene dysregulation in a Tet1 null mouse model is stochastic and variable in the germline and offspring. Development 145, dev.160622. 10.1242/dev.160622.

Sanz LA, Chamberlain S, Sabourin J, Henckel A, Magnuson T, Hugnot J, Feil R, and Arnaud P (2008). A mono-allelic bivalent chromatin domain controls tissue-specific imprinting at Grb10. Embo J 27, 2523–2532. 10.1038/emboj.2008.142. [PubMed: 18650936]

Schindelin J, Arganda-Carreras I, Frise E, Kaynig V, Longair M, Pietzsch T, Preibisch S, Rueden C, Saalfeld S, Schmid B, et al. (2012). Fiji: an open-source platform for biological-image analysis. Nat Methods 9, 676–682. 10.1038/nmeth.2019. [PubMed: 22743772]

Shah S, Henry A, Roselli C, Lin H, Sveinbjörnsson G, Fatemifar G, Hedman ÅK, Wilk JB, Morley MP, Chaffin MD, et al. (2020). Genome-wide association and Mendelian randomisation analysis provide insights into the pathogenesis of heart failure. Nat Commun 11, 163. 10.1038/s41467-019-13690-5. [PubMed: 31919418]

Shen W-J, Kong L-H, Chen S-L, Li H, and Xing F-Q (2005). Expression of imprinted gene Grb10 in human oocytes and preimplantation embryos. Academic Journal of the First Medical College of PLA (Di Yi Jun Yi Da Xue Xue Bao) 25, 305–307.. [PubMed: 15771999]

Shiura H, Nakamura K, Hikichi T, Hino T, Oda K, Suzuki-Migishima R, Kohda T, Kaneko-Ishino T, and Ishino F (2009). Paternal deletion of Meg1/Grb10 DMR causes maternalization of the Meg1/Grb10 cluster in mouse proximal Chromosome 11 leading to severe pre- and postnatal growth retardation. Hum Mol Genet 18, 1424–1438. 10.1093/hmg/ddp049. [PubMed: 19174477]

Singh VB, Sribenja S, Wilson KE, Attwood KM, Hillman JC, Pathak S, and Higgins MJ (2017). Blocked transcription through KvDMR1 results in absence of methylation and gene silencing resembling Beckwith-Wiedemann syndrome. Development 144, 1820–1830. 10.1242/dev.145136. [PubMed: 28428215]

Sleutels F, Zwart R, and Barlow DP (2002). The non-coding Air RNA is required for silencing autosomal imprinted genes. Nature 415, 810–813. 10.1038/415810a. [PubMed: 11845212]

Sloan CA, Chan ET, Davidson JM, Malladi VS, Strattan JS, Hitz BC, Gabdank I, Narayanan AK, Ho M, Lee BT, et al. (2016). ENCODE data at the ENCODE portal. Nucleic Acids Res 44, D726–D732. 10.1093/nar/gkv1160. [PubMed: 26527727]

Smith EY, Futtner CR, Chamberlain SJ, Johnstone KA, and Resnick JL (2011). Transcription Is Required to Establish Maternal Imprinting at the Prader-Willi Syndrome and Angelman Syndrome Locus. Plos Genet 7, e1002422. 10.1371/journal.pgen.1002422. [PubMed: 22242001]

Smith ZD, Chan MM, Mikkelsen TS, Gu H, Gnirke A, Regev A, and Meissner A (2012). A unique regulatory phase of DNA methylation in the early mammalian embryo. Nature 484, 339–344. 10.1038/nature10960. [PubMed: 22456710]

Spurrell CH, Barozzi I, Mannion BJ, Blow MJ, Fukuda-Yuzawa Y, Afzal SY, Akiyama JA, Afzal V, Tran S, Plajzer-Frick I, et al. (2019). Genome-Wide Fetalization of Enhancer Architecture in Heart Disease. Biorxiv 591362. 10.1101/591362.

Takada S, Tevendale M, Baker J, Georgiades P, Campbell E, Freeman T, Johnson MH, Paulsen M, and Ferguson-Smith AC (2000). Delta-like and Gtl2 are reciprocally expressed, differentially

methylated linked imprinted genes on mouse chromosome 12. Curr Biol 10, 1135–1138. 10.1016/s0960-9822(00)00704-1. [PubMed: 10996796]

Takada T, Ebata T, Noguchi H, Keane TM, Adams DJ, Narita T, Shin-I T, Fujisawa H, Toyoda A, Abe K, et al. (2013). The ancestor of extant Japanese fancy mice contributed to the mosaic genomes of classical inbred strains. Genome Res 23, 1329–1338. 10.1101/gr.156497.113. [PubMed: 23604024]

Thorvaldsen JL, Duran KL, and Bartolomei MS (1998). Deletion of the H19 differentially methylated domain results in loss of imprinted expression of H19 and Igf2. Genes & Development 12, 3693–3702. 10.1101/gad.12.23.3693. [PubMed: 9851976]

Tichy ED, Ma N, Sidibe D, Loro E, Kocan J, Chen DZ, Khurana TS, Hasty P, and Mourkioti F (2021). Persistent NF-κB activation in muscle stem cells induces proliferation-independent telomere shortening. Cell Reports 35, 109098. 10.1016/j.celrep.2021.109098. [PubMed: 33979621]

Tucci V, Isles AR, Kelsey G, Ferguson-Smith AC, Group, the E.I., Tucci V, Bartolomei MS, Benvenisty N, Bourc'his D, Charalambous M, et al. (2019). Genomic Imprinting and Physiological Processes in Mammals. Cell 176, 952–965. 10.1016/j.cell.2019.01.043. [PubMed: 30794780]

Tusnády GE, Simon I, Váradi A, and Arányi T (2005). BiSearch: primer-design and search tool for PCR on bisulfite-treated genomes. Nucleic Acids Res 33, e9–e9. 10.1093/nar/gni012. [PubMed: 15653630]

Veselovska L, Smallwood SA, Saadeh H, Stewart KR, Krueger F, Maupetit-Méhouas S, Arnaud P, Tomizawa S, Andrews S, and Kelsey G (2015). Deep sequencing and de novo assembly of the mouse oocyte transcriptome define the contribution of transcription to the DNA methylation landscape. Genome Biol 16, 209. 10.1186/s13059-015-0769-z. [PubMed: 26408185]

Wakeling EL, Brioude F, Lokulo-Sodipe O, O'Connell SM, Salem J, Bliek J, Canton APM, Chrzanowska KH, Davies JH, Dias RP, et al. (2017). Diagnosis and management of Silver–Russell syndrome: first international consensus statement. Nat Rev Endocrinol 13, 105–124. 10.1038/nrendo.2016.138. [PubMed: 27585961]

Wang H, Yang H, Shivalila CS, Dawlaty MM, Cheng AW, Zhang F, and Jaenisch R (2013). One-Step Generation of Mice Carrying Mutations in Multiple Genes by CRISPR/Cas-Mediated Genome Engineering. Cell 153, 910–918. 10.1016/j.cell.2013.04.025. [PubMed: 23643243]

Williams RL, Starmer J, Mugford JW, Calabrese JM, Mieczkowski P, Yee D, and Magnuson T (2014). fourSig: a method for determining chromosomal interactions in 4C-Seq data. Nucleic Acids Res 42, e68–e68. 10.1093/nar/gku156. [PubMed: 24561615]

Yang B, Damaschke N, Yao T, McCormick J, Wagner J, and Jarrard D (2015). Pyrosequencing for Accurate Imprinted Allele Expression Analysis. J Cell Biochem 116, 1165–1170. 10.1002/jcb.25081. [PubMed: 25581900]

Yang H, Wang H, and Jaenisch R (2014). Generating genetically modified mice using CRISPR/Cas-mediated genome engineering. Nat Protoc 9, 1956–1968. 10.1038/nprot.2014.134. [PubMed: 25058643]

Yavarone MS, Shuey DL Dr., Tamir H, Sadler TW, and Lauder JM Dr. (1993). Serotonin and Cardiac Morphogenesis in the Mouse Embryo. Teratology 47, 573–584.. [PubMed: 8367830]

Yuan H, Huang L, Hu X, Li Q, Sun X, Xie Y, Kong S, and Wang X (2016). FGFR3 gene mutation plus GRB10 gene duplication in a patient with achondroplasia plus growth delay with prenatal onset. Orphanet J Rare Dis 11, 89. 10.1186/s13023-016-0465-4. [PubMed: 27370225]

Zhang D, Huang P, Sharma M, Keller CA, Giardine B, Zhang H, Gilgenast TG, Phillips-Cremins JE, Hardison RC, and Blobel GA (2020). Alteration of genome folding via contact domain boundary insertion. Nat Genet 52, 1076–1087. 10.1038/s41588-020-0680-8. [PubMed: 32868908]

Zhou P, Gu F, Zhang L, Akerberg BN, Ma Q, Li K, He A, Lin Z, Stevens SM, Zhou B, et al. (2017). Mapping cell type-specific transcriptional enhancers using high affinity, lineage-specific Ep300 bioChIP-seq. Elife 6, e22039. 10.7554/elife.22039. [PubMed: 28121289]

Highlights:

- Maternal *Grb10* suppresses growth, while paternal *Ddc* stimulates heart development
- Intronic, maternally methylated CBR2.3 binds CTCF on the paternal allele
- CBR2.3 is a tissue and allele-specific CTCF-dependent insulator for a heart enhancer
- Paternal CBR2.3 deletion phenocopies the maternal allele, impairing heart growth

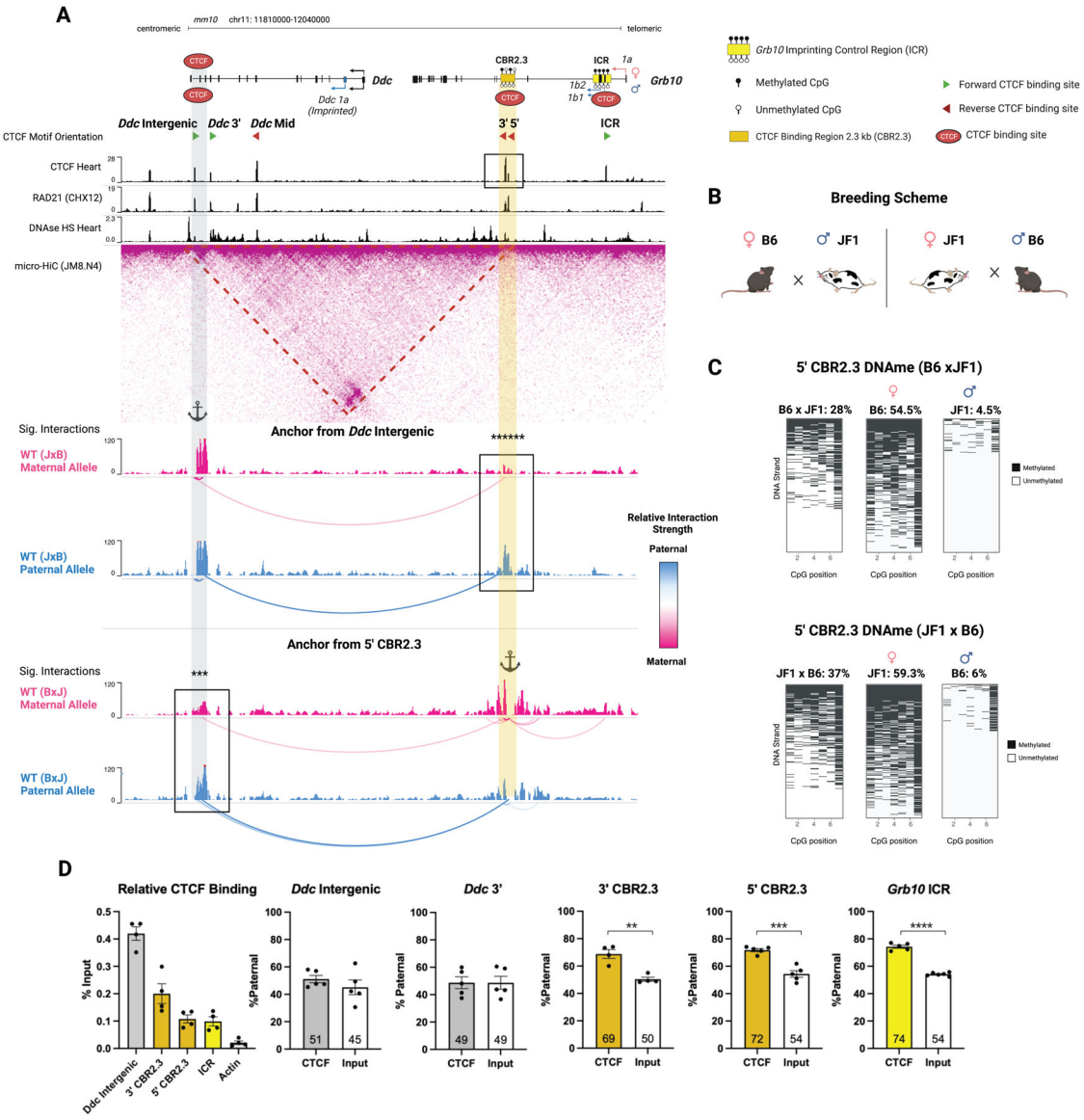

Figure 1: Analysis of CTCF binding sites at the *Grb10-Ddc* locus.

(A) *Grb10* is transcribed from exon *1a* on the maternal allele and exons *1b1/1b2* (within the ICR) on the paternal allele. CBR2.3 is located within the intron after common exon 2. CTCF binding regions and motif polarity are depicted above the WashU Epigenome Browser tracks of Public ENCODE and 4D Nucleome Network data (Supp. Table 1), revealing a ~150 kb interaction between CBR2.3 (orange) and *Ddc* (grey) CTCF binding sites. Below, our normalized Capture-C interaction frequencies in F1 hybrid neonatal hearts are shown from the viewpoints of 5' CBR2.3 and *Ddc* Intergenic CTCF. Probe locations are indicated by anchors. Pink and blue tracks refer to the maternal and paternal alleles, respectively, with darker intensities corresponding to stronger interactions. ****** *Wald statistic* $p<10^{-6}$ for *Ddc* Intergenic-CBR2.3 and ***$p<10^{-3}$ for 5'CBR2.3-*Ddc* Intergenic interactions, respectively (Supp. Table 5). **(B)** Mouse breeding scheme to generate reciprocal F1 hybrids. **(C)** Allele-specific DNA methylation analysis for 5' CBR2.3 in reciprocal

neonate F1 hybrid livers. **(D)** Total and allele-specific CTCF ChIP-qPCR for F1 neonatal liver revealed preferential paternal CTCF binding to CBR2.3 and ICR ($n = 4–5$) and two-way Student's *t* test ****$p<0.0001$; ***$p<0.001$; **$p<0.01$; *$p<0.05$).

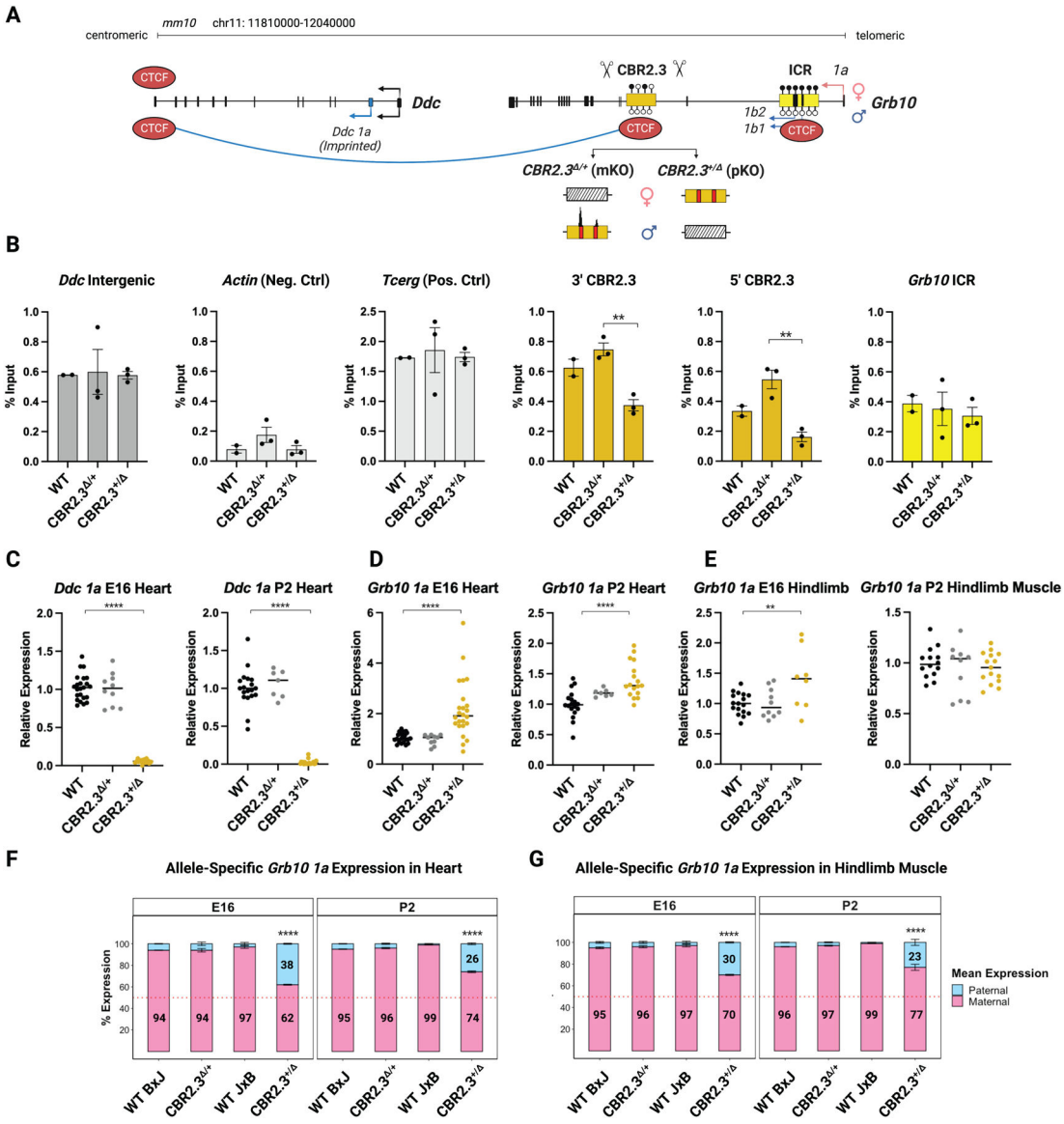

Figure 2: Deletion of paternal CBR2.3 perturbs *Grb10* and *Ddc* expression in muscle tissues.

(**A**) The *Grb10-Ddc* locus and CBR2.3 KO mouse model. **(B)** CTCF-ChIP qPCR on mutant P2 heart (n = 2–3 WT, $CBR2.3^{\Delta/+}$ and $CBR2.3^{+/\Delta}$). **(C)** Total *Ddc 1a* expression in E16 and P2 WT, $CBR2.3^{+/\Delta}$ and $CBR2.3^{\Delta/+}$ heart. **(D)** Total *Grb10 1a* expression in E16 and P2 WT, $CBR2.3^{\Delta/+}$ and $CBR2.3^{+/\Delta}$ heart and (**E**) hindlimb muscle. **(F-G)** Allele-specific RT-PCR followed by pyrosequencing for *Grb10 1a* expression in $CBR2.3^{+/\Delta}$ in E16 and P2 heart and muscle. For total expression heart studies: n = 23 WT (8 litters), 10 $CBR2.3^{\Delta/+}$ (4 litters), 17 $CBR2.3^{+/\Delta}$ (4 litters) (E16); n = 19 WT (9 litters), 7 $CBR2.3^{\Delta/+}$ (3 litters), 17 $CBR2.3^{+/\Delta}$ (6 litters) (P2). For total expression hindlimb studies: n = 7 WT (2 litters), n = *9* $CBR2.3^{\Delta/+}$ (3 litters), n = 8 $CBR2.3^{+/\Delta}$ (2 litters) (E16); n = 17 WT (6 litters), n = 10 $CBR2.3^{\Delta/+}$ (3 litters), n = 15 $CBR2.3^{+/\Delta}$ (4 litters) (P2). For E16 allelic expression studies: n = 3 WT JxB (3 litters); n = *7* BxJ (3 litters); n = 6 $CBR2.3^{+/\Delta}$ JxB (4 litters); n = 7 $CBR2.3^{\Delta/+}$ BxJ (from 3 litters). For P2 allelic expression studies: n = *9* WT JxB: (4 litters); n = *12* WT BxJ: (4

litters); *n = 11 CBR2.3*$^{+/\Delta}$ JxB (6 litters); *n* = 12 *CBR2.3*$^{\Delta/+}$ BxJ (4 litters*)*. Statistics for (**B**): For groups where *n* =3, a two-sided Student's *t*-test was used: ***p*<0.005; **p*<0.05. (**C**-**E**): One-way ANOVA followed by Tukey's multiple comparisons post-hoc test: *****p*<0.0001. Statistics for **F**-**G**: Two-way ANOVA, *****p*<0.0001.

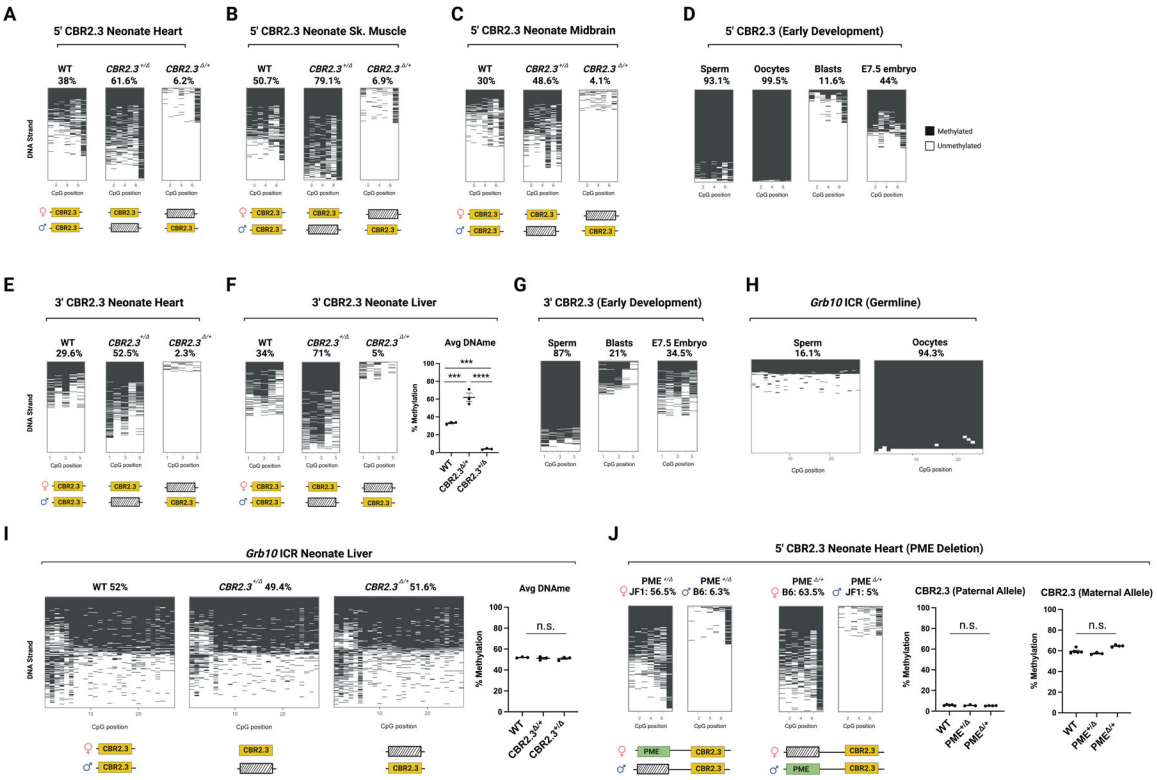

Figure 3: Allelic DNA methylation profile of CBR2.3 and PME.

(**A-C**) Targeted bisulfite sequencing for 5' and 3' CBR2.3 in WT, *CBR2.3*$^{\Delta/+}$ and *CBR2.3*$^{+/\Delta}$ neonatal heart, skeletal muscle and midbrain. Representative heatmaps (n = 2) depicting the preferentially methylated maternal allele and hypomethylated paternal allele (>1000 reads/animal). (**D**) 5' CBR2.3 is hypermethylated in gametes. DNA methylation is erased in blastocysts but is regained by E7.5. (**E-G**) Repeat studies for 3' CBR2.3 in WT, *CBR2.3*$^{\Delta/+}$ and *CBR2.3*$^{+/\Delta}$ tissues. (**H**) *Grb10* ICR DNA methylation for reference. (**I**) Representative heatmaps for DNA methylation at the *Grb10* ICR in WT, *CBR2.3*$^{\Delta/+}$ and *CBR2.3*$^{+/\Delta}$ P2 liver. *Right:* Average DNA methylation plotted for each genotype. (**J**) Allele-specific methylation of CBR2.3 in neonatal PME mutant hearts.

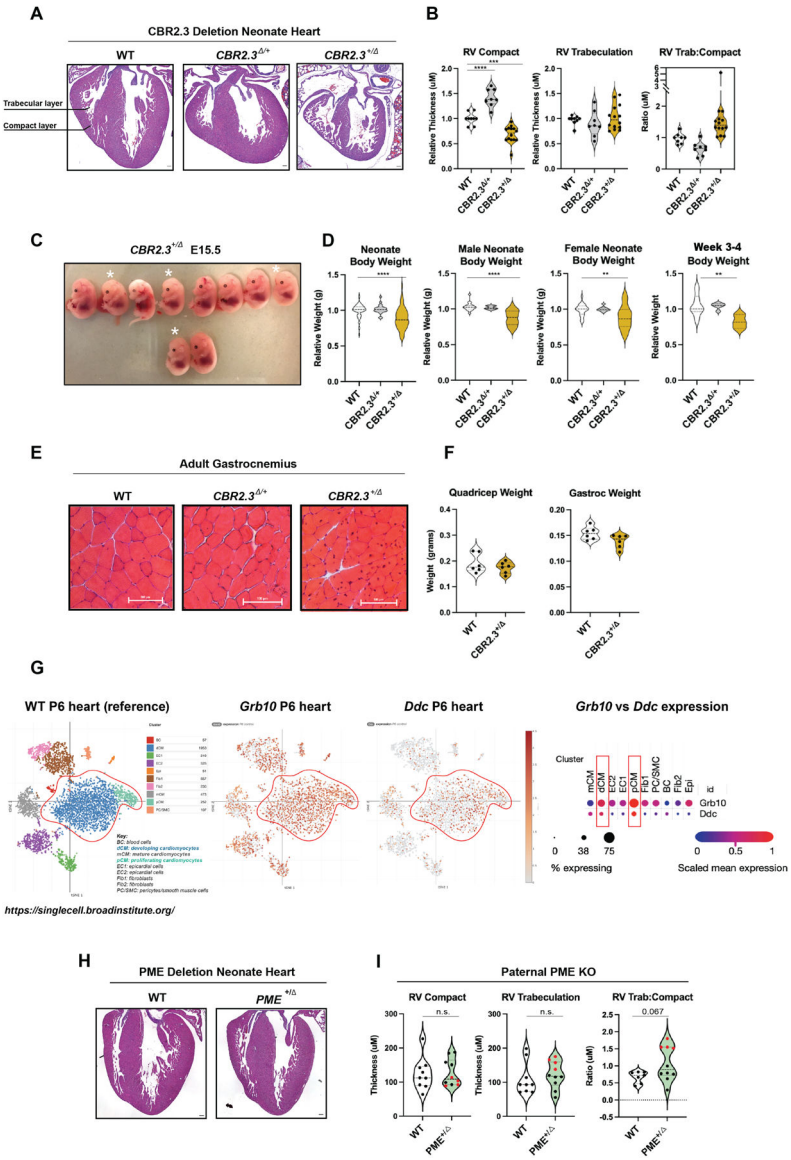

Figure 4: Phenotypic analyses in mutant CBR2.3 and PME mice.

(**A**) Representative images of right ventricular wall thinning in *CBR2.3*$^{+/\Delta}$ P2 hearts using hematoxylin and eosin staining **(B)** Quantification of the compact and trabecular cardiac wall thicknesses, including compact:trabecular wall ratio of the right ventricle (measured in *u*M, all measurements are relative to WT littermates). *n* = 9 WT (7 litters); *n* = 8 *CBR2.3*$^{\Delta/+}$ (3 litters); *n* = 14 *CBR2.3*$^{+/\Delta}$ (4 litters). **(C)** Representative image of *CBR2.3*$^{+/\Delta}$ E15.5 embryos labeled with a white asterisk (*). **(D)** Neonatal body weight relative to WT littermates. *n* = 64 WT (17 litters); *n* = 54 *CBR2.3*$^{+/\Delta}$ (11 litters); *n* = 24 *CBR2.3*$^{\Delta/+}$ (6 litters). Adult body weight relative to WT littermates, *n* = 6 WT (5 litters); *n* = 5 *CBR2.3*$^{\Delta/+}$ (2 litters); *n* = 3 *CBR2.3*$^{+/\Delta}$ (3 litters). (**E**) Centralized nuclei in myofibers of *CBR2.3*$^{+/\Delta}$, at 6–12 months, *n* = 2 for each genotype. (**F**) Weight of dissected adult quadricep and gastrocnemius muscles. (**G**) Publicly available scRNA-seq data available from the Broad Institute (https://singlecell.broadinstitute.org), obtained from Hu et al., *Genes & Dev* (2018).

P6 mouse hearts separate into at least 9 cell types. *Grb10* and *Ddc* are co-expressed in developing and proliferating cardiomyocytes. Dot plot analyses depict percentage of expressing cells, with larger circles representing higher abundance, and scaled mean of each gene's expression across all cells of a given cell type are represented by blue (weakly expressed) or red (highly expressed). (**H**) Representative WT and $PME^{+/\Delta}$ neonate hearts. (**I**) No statistical difference in heart measurements between groups. Animals with greater levels of trabeculation are highlighted in red. Statistics: For $n \geq 3$ groups, one-way ANOVA followed by Tukey's multiple comparisons post-hoc test: ****p<0.0001; ***p<0.001. Violin plots depict median, 25th and 75th quartiles. For $n = 2$ groups, a two-tailed Student's *t*-test was used, p<0.05. Scale bar = 245 uM.

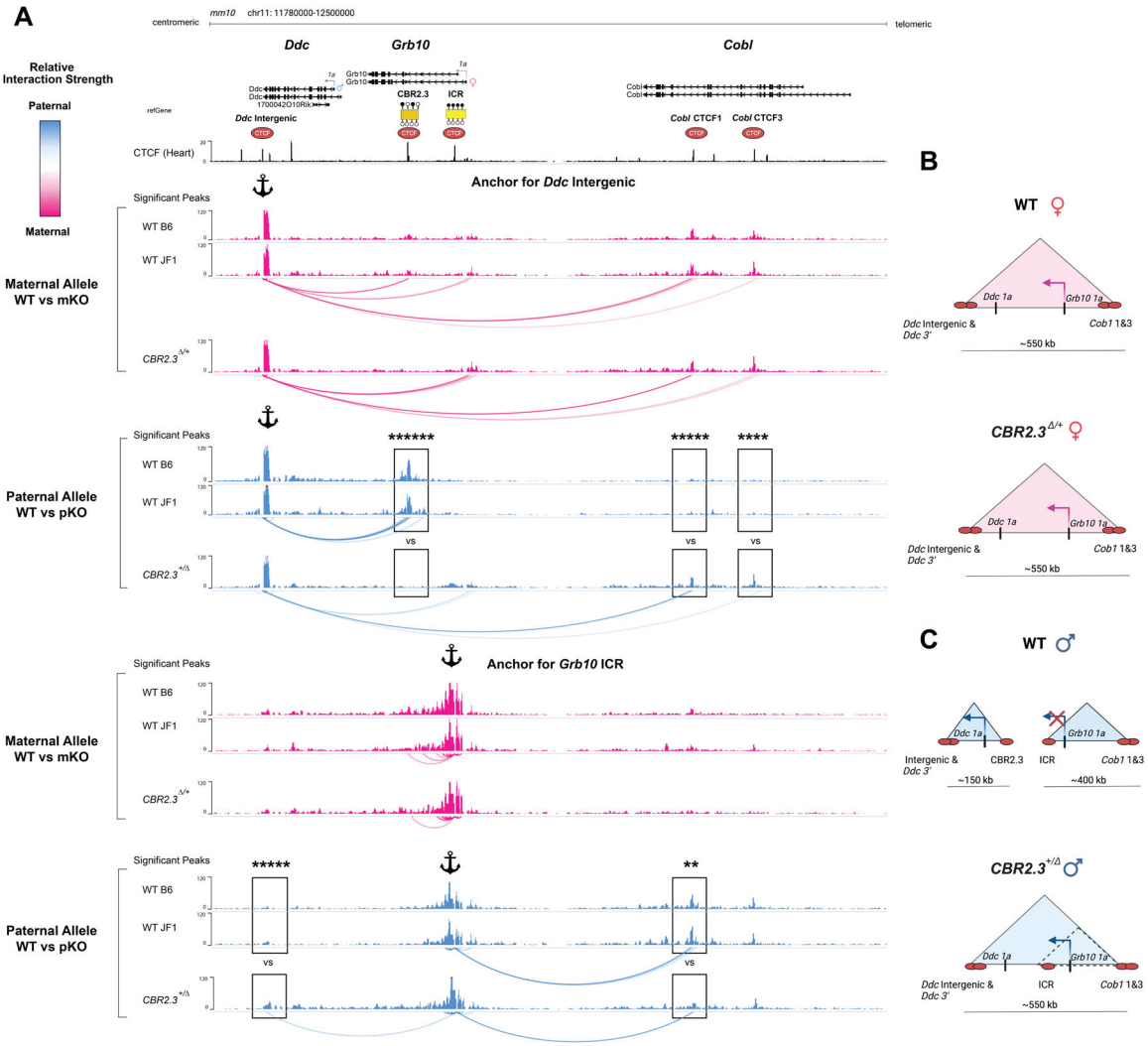

Figure 5: Allelic looping interaction from *Ddc-Grb10* to *Cobl*.

(**A**) *Ddc-Grb10-Cobl* locus CTCF binding sites (Supp Table 1) are depicted above representative, normalized Capture-C tracks for WT BxJ, WT JxB, $CBR^{\Delta/+}$ and $CBR2.3^{+/\Delta}$ neonate heart and combined arcs (n =3 for each genotype) using *Ddc* Intergenic and *Grb10* ICR as viewpoints (anchor). Ectopic paternal-specific *Ddc* Intergenic-*Cobl1 & 3* interactions are gained in $CBR2.3^{+/\Delta}$ compared to WT (Wald statistic, ***** $p<10^{-5}$ and **** $p<10^{-4}$, respectively). Paternal-specific interactions between *Ddc* Intergenic and CBR2.3 are lost in CBR2.3$^{+/\Delta}$ mutants, shown in blue arcs (WT paternal vs CBR2.3$^{+/\Delta}$ paternal alleles: Wald statistic ****** $p<10^{-6}$). Paternal ICR interacts with *Cobl* CTCF sites only on the paternal allele (WT paternal vs WT maternal allele ICR-*Cobl1&3*: Wald statistic $p<0.001$ and $p<10^{-4}$, respectively. Supp Table 5). $CBR2.3^{+/\Delta}$ hearts display weakened ICR-*Cobl* interactions compared to WT (** $p < 0.01$) and increased interactions with *Ddc* Intergenic (***** $p<10^{-5}$). All Capture-C statistics are provided in Supp. Table 5. (**B-C**) Model for the allele-specific architecture across *Grb10-Ddc-Cobl* locus in WT and CBR2.3 mutants. The WT maternal allele forms a ~550 kb domain bounded by CTCF at *Ddc* Intergenic and *Cobl*. The WT paternal allele is divided into two subdomains: *Ddc* Intergenic-CBR2.3 and

ICR-*Cobl* 1 & 3. Maternal CBR2.3 deletion does not change architecture. Paternal CBR2.3 deletion causes the paternal allele to adopt maternal architecture, with silencing of paternal *Ddc 1a* and activation of *Grb10 1a* promoters in heart.

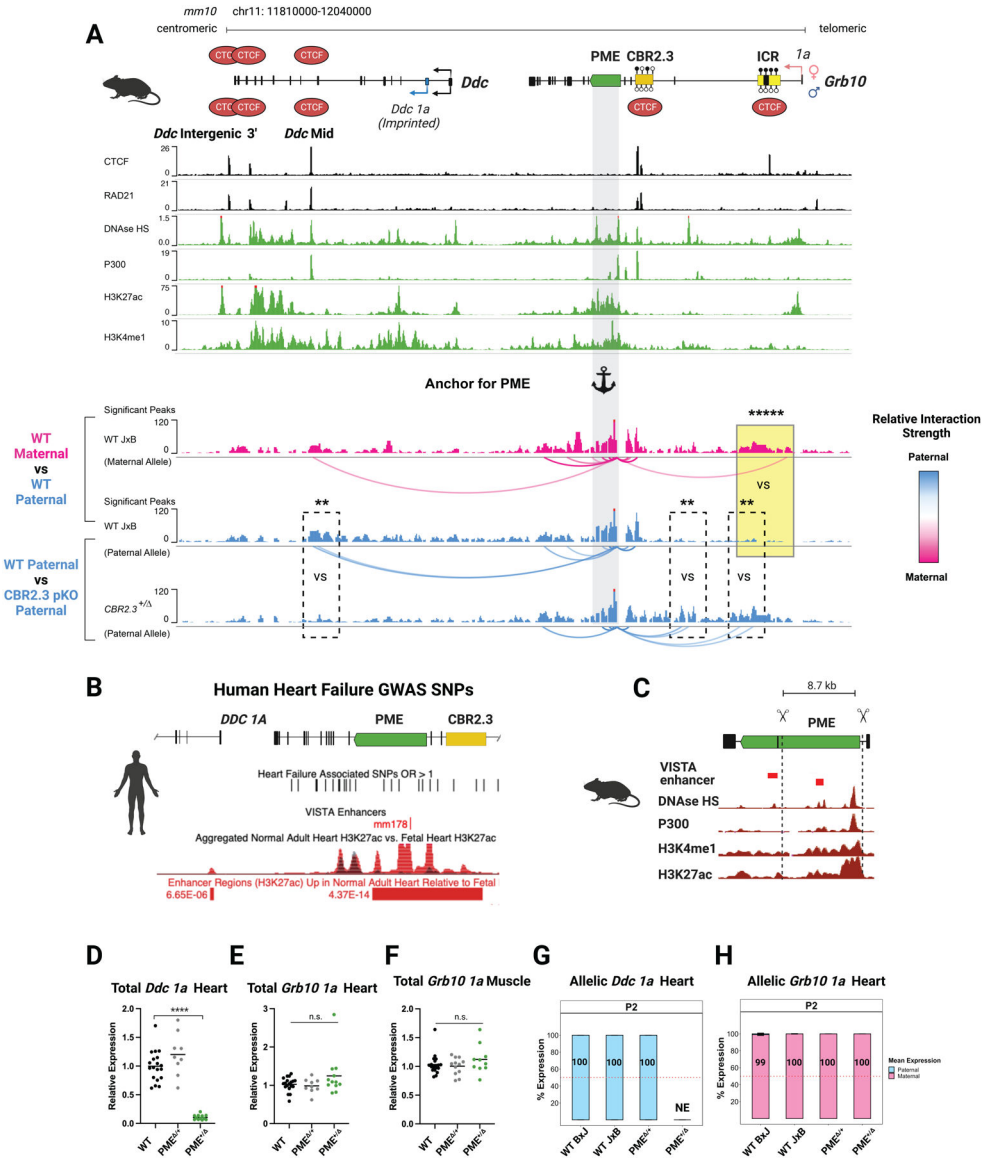

Figure 6: Characterization of heart-specific enhancer, PME.

(**A**) Schematic of PME is highlighted in gray. ChIP-Seq enhancer marks for embryonic heart are shown in green. Normalized Capture-C tracks for allele-specific interactions originating from PME (anchor) in WT JxB and *CBR2.3*$^{+/\Delta}$ hearts are shown. Pink and blue arcs of varying intensities depict the strength of maternal- and paternal-specific contacts, respectively. Yellow box: WT maternal allele vs WT paternal allele PME-*Grb10* promoter region, Wald statistic *****$p<10^{-5}$. Dotted boxes: WT paternal allele vs *CBR2.3*$^{+/\Delta}$ paternal allele, PME-*Grb10* promoter region: Wald statistic, **$p<0.01$). Statistics provided in Supp. Table 5. (**B**) Conserved enhancer marks localize to PME in human, and SNPs with OR >1 within PME increase risk of heart failure. (**C**) Schematic of deleted PME sequence in mice using CRISPR/Cas9. **(D-F)** Total *Ddc 1a* and *Grb10 1a* expression with maternal and paternal inheritance of PME deletion (heart: $n = 19$ WT, n=9 PME$^{\Delta/+}$, $n = 12$ PME$^{+/\Delta}$, from 2–3 litters; muscle: $n = 20$ WT, $n = 12$ PME$^{\Delta/+}$, $n = 10$ PME$^{+/\Delta}$ from 3–4 litters). (**G-H**)

Allelic *Grb10* 1a and *Ddc 1a* expression in neonate hearts derived from reciprocal J11 × PME reciprocal crosses (n = 6 WT: 3 BxJ, 3 JxB; n = 5 $PME^{\Delta/+}$; n = 2 $PME^{+/\Delta}$; 1–2 litters). Accession numbers for all public data tracks are provided in Supp. Table 1.

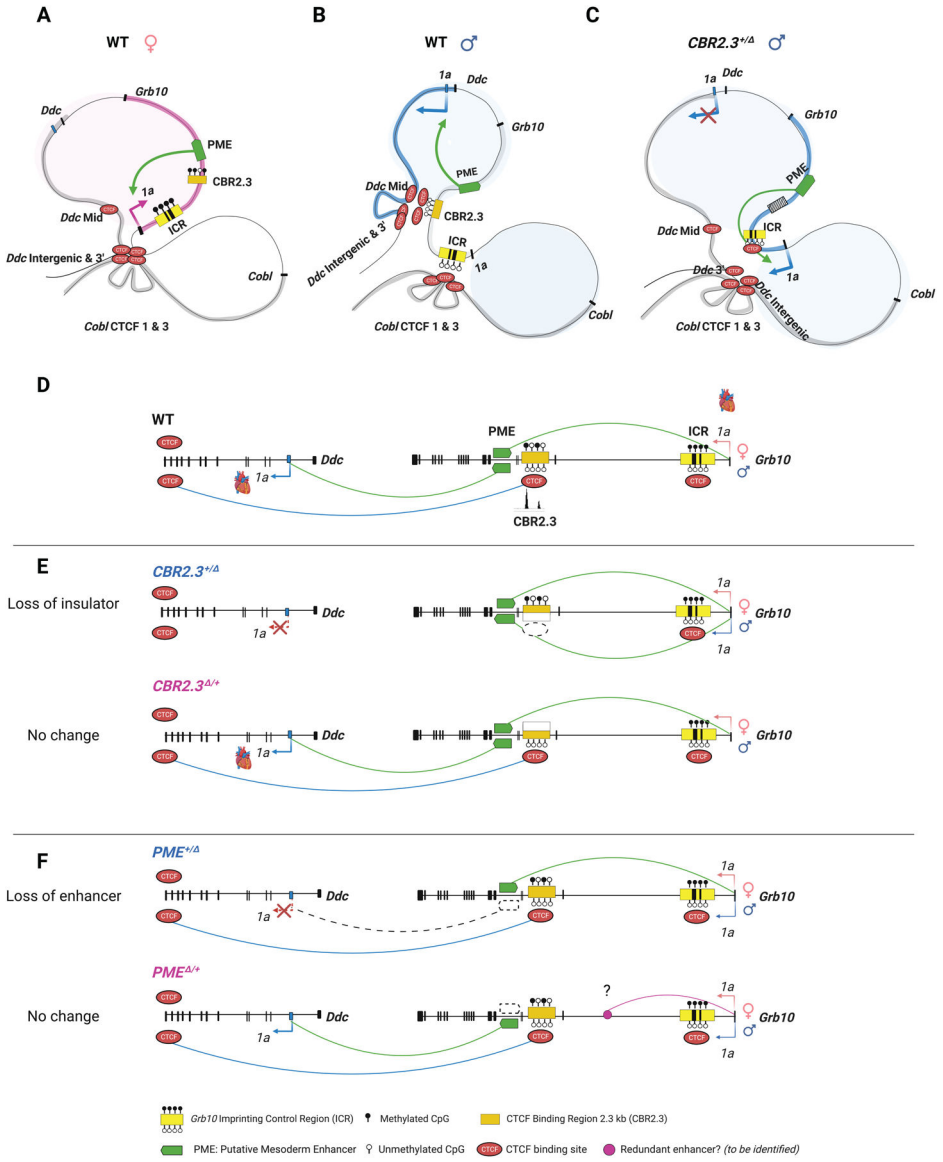

Figure 7: Looping model of interactions for *Grb10-Ddc-Cobl* locus for each parental allele.

(A) WT maternal allele. **(B)** WT paternal allele. (**C**) Paternal deletion of CBR2.3 reorganizes architecture that mimics maternal allele. (**D**) Stick model for regulatory elements and their targets at the WT *Grb10-Ddc* locus. (**E**) Deletion of paternal and maternal CBR2.3 and resulting changes in interactions/gene expression. (**F**) Deletion of paternal and maternal PME and resulting changes.

Key resources table

REAGENT or RESOURCE	SOURCE	IDENTIFIER
Antibodies		
CTCF (D31H2) XP Rabbit mAb	Cell Signaling Technology	Cat# 3418; RRID:AB_2086791
ChromPure Rabbit IgG	Jackson ImmunoResearch	Cat# 011-000-003 RRID:AB_2337118
Histone H3K27ac Rabbit pAb	Active Motif	Cat# 39133 RRID:AB_2561016
Chemicals, peptides, and recombinant proteins		
KSOM media	Millipore	MR-020P-5F
mineral oil	Millipore	ES-005-C
CZB-HEPES	Millipore	MR-019-D
M2 medium	Sigma-Aldrich	M7167
Proteinase K	Sigma-Aldrich	P2308
Phenol:Chloroform:Isoamyl Alcohol	Sigma-Aldrich	P3803
Critical commercial assays		
Phusion HF PCR Kit	NEB	E0553S
HiScribe T7 Quick High Yield RNA Synthesis Kit	NEB	E2040S
MEGAclear Transcription Clean-up Kit	Ambion	AM1908
Agilent RNA 6000 Nano Kit	Agilent	5067-1511
GoTaq Green Master Mix	Promega	M7121
Epitect Bisulfite Kit	Qiagen	59104
Epitect Fast Bisulfite Conversion Kit	Qiagen	59824
PyroMark PCR kit	Qiagen	978703
Multiplex PCR Kit	Qiagen	246145
Bioanalyzer DNA High Sensitivity Chip	Agilent	5067-4626
MiSeq Reagent Nano Kit v2 (500 cycles)	Illumina	MS-102-2003
xGen Prism DNA library kit with primers and adapters	IDT	10006202, 10005975, 10006914
xGen Hybridization and Wash Kit	IDT	1080577
Nova-Seq 600 SP reagent kit v1.5 (500 cycles)	Illumina	20028402
Nova-Seq Xp 2-Lane kit v1.5	Illumina	20043130
KAPA HiFi HotStart Readymix Kit	KAPA Biosystems	KR0370
Library amplification primer	IDT	1077676
Deposited data		
Mouse Public Data Table S1	This paper	N/A
Human Public Data Table S1	This paper	N/A
Raw Capture C data	This paper	GSE201519
Human GWAS HS SNP's Table S4	https://cvd.hugeamp.org/	N/A

REAGENT or RESOURCE	SOURCE	IDENTIFIER
Mendeley Data	This paper	https://data.mendeley.com/datasets/vmgpf62kxz/draft?a=3458285f-4067-417dbc21-265ddc2f4065
Experimental models: Organisms/strains		
Mouse: C57BL/6J (B6)	JAX	Strain# 000664 RRID:IMSR_JAX:000664
Mouse: DBA/2J	JAX	Strain# 000671 RRID:IMSR_JAX:000671
Mouse: Hsd:NSA (CF-1)	ENVIGO	Strain Code# 033
Mouse: Swiss Webster (CFW)	Charles River	Strain Code# 024
Mouse: JF1/MsJ (JF1)	JAX	Strain# 003720 RRID:IMSR_JAX:003720
Mouse: J11	This paper	N/A
Mouse: *Grb10*^{em1msb} (CBR2.3 deletion)	This paper	N/A
Mouse: *Grb10*^{em2msb} (PME deletion)	This paper	N/A
Oligonucleotides		
Primers for Total CTCF and H3K27ac ChIP qPCR, see Table 2.1	This paper	N/A
Primers for Allele-Specific CTCF H3K27ac ChIP, see Table 2.2	This paper	N/A
Primers for Targeted Bisulfite Sequencing, see Table 2.3	This paper	N/A
Primers for Mouse CRISPR sgRNAs, see Table 2.4	This paper	N/A
Primers for Southern blot probes, see Table 2.5	This paper	N/A
Primers for Genotyping, see Table 2.6	This paper	N/A
Primers for Expression (rt-qPCR), see Table 2.7	This paper	N/A
Primers for Allele-Specific expression, see Table 2.8	This paper	N/A
Capture-C probes, see Table 3.1	This paper	N/A
Software and algorithms		
PWMScan- Genome Position Weight Matrix (PWM) scanner	(Ambrosini et al., 2018)	https://ccg.epfl.ch/pwmscan/
MethPrimer	(Li and Dahiya, 2002)	https://www.urogene.org/methprimer/)(
BiSearch	(Tusnády et al., 2005)	http://bisearch.enzim.hu/
Trim Galore (version 0.6.2)	Felix Krueger: DOI:10.14806/ej.17.1.200 NBIS (National Bioinformatics Infrastructure Sweden)	https://github.com/FelixKrueger/TrimGalore
Cutadapt version 2.3	Felix Krueger: DOI:10.14806/ej.17.1.200 NBIS (National Bioinformatics Infrastructure Sweden)	https://cutadapt.readthedocs.io/en/stable/
IMPLICON pipeline	(Klobučar et al., 2020)	https://github.com/FelixKrueger/IMPLICON#step-i-umihandling
SNPsplit package, version 0.3.4	(Krueger and Andrews, 2016)	https://github.com/FelixKrueger/SNPsplit

REAGENT or RESOURCE	SOURCE	IDENTIFIER
Bismark version 0.22.3	(Krueger and Andrews, 2011)	https://www.bioinformatics.babraham.ac.uk/projects/bismark
Prism 9	GraphPad	N/A
ImageJ 1.52k	ImageJ	N/A
PyroMark Q96 MD Pyrosequencer	Biotage AB	N/A
FIJI v2.0.0	(Schindelin et al., 2012)	https://imagej.net/software/fiji/#publication
Pyrosequencing for Imprinting Expression (PIE)	(Calabrese et al., 2015; Yang et al., 2015)	N/A
RStudio (v1.4)	RStudio Team (2020). RStudio: Integrated Development for R. RStudio, PBC, Boston, MA	http://www.rstudio.com/.
CCseqBasicS pipeline	(Downes et al., 2021)	https://github.com/Hughes-Genome-Group/CCseqBasicS
fgbio toolkit (v0.5.0a)	Fulcrumgenomics	https://github.com/fulcrumgenomics/fgbio
BWA MEM (v0.7.17)	(Li, 2013)	http://bio-bwa.sourceforge.net/bwa.shtml
FLASH (v1.2.11)	(Magoč and Salzberg, 2011)	http://ccb.jhu.edu/software/FLASH/
Bowtie (version 2.3.4.3)	(Langmead, 2010)	http://bowtiebio.sourceforge.net/bowtie2/index.shtml
fourSig	(Williams et al., 2014)	https://sourceforge.net/projects/foursig/
bwtool (v1.0)	(Pohl and Beato, 2014)	https://github.com/CRG-Barcelona/bwtool/wiki
DESeq2 R package (FDR 0.05)	(Love et al., 2014)	https://bioconductor.org/packages/release/bioc/html/DESeq2.html
Other		
Quick-RNA Miniprep Plus	ZYMO	R1057
Superscript IV reverse transcriptase	Invitrogen	18090010
Power SYBR Green master mix	Applied Biosystems	A46111
Apex Taq RED Master Mix	Apex Bioresearch Products	42–138
PyroMark Gold Q96 CDT Reagents	Qiagen	972824
Streptavidin Sepharose beads	GE Healthcare	GE17-5113-01